Improving High-Resolution Weather Forecasts Using the Weather Research and Forecasting (WRF) Model with an Updated Kain–Fritsch Scheme

YUE ZHENG

Department of Earth, Atmospheric, and Planetary Sciences, Purdue University, West Lafayette, Indiana

KIRAN ALAPATY AND JEROLD A. HERWEHE

National Exposure Research Laboratory, U.S. Environmental Protection Agency, Research Triangle Park, North Carolina

ANTHONY D. DEL GENIO

NASA Goddard Institute for Space Studies, New York, New York

DEV NIYOGI

Department of Agronomy, and Department of Earth, Atmospheric, and Planetary Sciences, Purdue University, West Lafayette, Indiana

(Manuscript received 17 December 2014, in final form 4 May 2015)

ABSTRACT

Efforts to improve the prediction accuracy of high-resolution (1–10 km) surface precipitation distribution and variability are of vital importance to local aspects of air pollution, wet deposition, and regional climate. However, precipitation biases and errors can occur at these spatial scales due to uncertainties in initial meteorological conditions and/or grid-scale cloud microphysics schemes. In particular, it is still unclear to what extent a subgrid-scale convection scheme could be modified to bring in scale awareness for improving high-resolution short-term precipitation forecasts in the WRF Model. To address these issues, the authors introduced scale-aware parameterized cloud dynamics for high-resolution forecasts by making several changes to the Kain–Fritsch (KF) convective parameterization scheme in the WRF Model. These changes include subgrid-scale cloud–radiation interactions, a dynamic adjustment time scale, impacts of cloud updraft mass fluxes on grid-scale vertical velocity, and lifting condensation level–based entrainment methodology that includes scale dependency.

A series of 48-h retrospective forecasts using a combination of three treatments of convection (KF, updated KF, and the use of no cumulus parameterization), two cloud microphysics schemes, and two types of initial condition datasets were performed over the U.S. southern Great Plains on 9- and 3-km grid spacings during the summers of 2002 and 2010. Results indicate that 1) the source of initial conditions plays a key role in high-resolution precipitation forecasting, and 2) the authors' updated KF scheme greatly alleviates the excessive precipitation at 9-km grid spacing and improves results at 3-km grid spacing as well. Overall, the study found that the updated KF scheme incorporated into a high-resolution model does provide better forecasts for precipitation location and intensity.

1. Introduction

Numerical weather prediction (NWP) forecast models have been greatly improved, motivated by the role of providing accurate forecasts about severe weather events to mitigate the loss of life and property. Furthermore, credibility of climate change simulations at urban scales can be increased by first improving the accuracy of high-resolution model simulations at weather prediction time scales (Chen et al. 2011). In particular, moist processes play an important role in properly simulating weather, air pollution, climate, and the hydrological cycle. Clouds and precipitation formed in these processes are important forecast products, thus accurate prediction of

Corresponding author address: Kiran Alapaty, U.S. Environmental Protection Agency, Mail Code E243-01, Research Triangle Park, NC 27711.
E-mail: alapaty.kiran@epa.gov

DOI: 10.1175/MWR-D-15-0005.1

precipitation is one of the most beneficial areas of NWP improvement. For this reason, key processes occurring within clouds, including microphysical and dynamical processes, need to be well understood and modeled.

Cloud microphysics schemes have been used in NWP models, but those microphysical processes may not be accurately represented due to the lack of supporting measurements for many processes occurring at finer spatial and temporal scales. For example, the formulation described in Kain et al. (2008) has been found to be appropriate for the Weather Research and Forecasting (WRF) single-moment 6-class microphysics scheme (WSM6; Hong et al. 2004) and has been successfully used in some numerical studies (e.g., Done et al. 2004; Deng and Stauffer 2006; Wulfmeyer et al. 2006; Case et al. 2008; Niyogi et al. 2011). However, according to Clark et al. (2012), many such studies are not able to accurately clarify unique precipitation particle and other physical parameters in different microphysical processes using regional models such as the WRF Model (Skamarock and Klemp 2008). This problem revealed that many characteristics of the model results were quite sensitive to the choice of microphysics scheme (Weisman et al. 2008; Dawson et al. 2010; Bryan and Morrison 2012). Clark et al. (2012) also found that no single microphysics scheme could surpass the others in performance during the 2010 National Oceanic and Atmospheric Administration's (NOAA's) Hazardous Weather Testbed (HWT) Spring Forecasting Experiment. There is also much debate on whether more complex microphysics schemes provide value for precipitation forecasts (e.g., Luo et al. 2010; Seifert and Stevens 2010; van Lier-Walqui et al. 2012; Van Weverberg et al. 2013). Based on the microphysics scheme sensitivity study of Blossey et al. (2007), microphysics was found to have little impact on decreasing a model's apparently excessive precipitation efficiency. Additionally, Cintineo et al. (2014) pointed out that large uncertainties remain in how various microphysics schemes represent subgrid-scale microphysical processes. Thus, as grid spacing decreases, cloud microphysics schemes have limitations in representing moist convection (Arakawa and Jung 2011; Gustafson et al. 2013; Molinari and Dudek 1992).

One reason for the partial failure of cloud microphysics schemes can be attributed to the fact that grid-scale dynamics is separated from cloud physics. Additionally, there will be clouds that are unresolved by high spatial resolutions (e.g., ~1–10-km grid spacings) and their effects need to be accounted for to improve predictability (e.g., Molinari and Dudek 1992; Seaman et al. 1998). Thus, from these studies it can be inferred that, at high spatial resolutions, usage of a cloud microphysics scheme alone (without an active parameterized convective scheme) may not be sufficient to represent moist convection and precipitation for warmer periods in weather forecasts.

The dynamic cloud processes that describe cloud formation and growth can impact the timing, location, and intensity of precipitation. In many NWP models, the fractional cloudiness can influence atmospheric radiation budgets as well as the dynamics and thermodynamics, but in the past, subgrid-scale cumulus cloudiness and the associated radiative impacts have been largely neglected outside of global climate models. Alapaty et al. (2012) and Herwehe et al. (2014) emphasized and documented the importance of incorporating such subgrid-scale cloud–radiation interactions using the Kain–Fritsch (KF) convective parameterization scheme (Kain 2004) and the Rapid Radiative Transfer Model for GCMs (RRTMG) schemes (Iacono et al. 2008). To represent subgrid-scale clouds at higher resolutions, it will be shown that there is a need to relax some of the assumptions used in convective parameterizations (e.g., the KF scheme). We address some of these issues that cause convective parameterization schemes to degrade progressively as resolution is increased, in particular for high-resolution modeling (for grid spacings on the order of 1–10 km).

One of the many key parameters in convective parameterization schemes is the convective adjustment time scale, a characteristic time scale with which convective available potential energy (CAPE) is reduced at an exponential rate by convection. This parameter is set as a constant value in many regional and global models with the exception of a very few models (e.g., the European Centre for Medium-Range Weather Forecasts model; Bechtold et al. 2008). Literature indicated that there is some uncertainty in the specification of this parameter. For example, Mishra and Srinivasan (2010) improved the simulation of the seasonal mean precipitation significantly by increasing the adjustment time scale value from 1 to 8 h, while Done et al. (2006) found that varying the adjustment time scale from minutes to 1 day resulted in changing all convective parameterization-generated subgrid-scale rainfall to only grid-scale precipitation. In addition, the magnitude of convective heating and drying rates has been found to correlate with local CAPE more strongly at finer scales when grid spacing is on the order of 1–10 km (Kain 2004). Another key cloud process is the interaction between convection and its environment through entrainment and detrainment. These processes are quite complex and are of vital importance in regional and global models (e.g., Tokioka et al. 1988; Kain and Fritsch 1990; Kang et al.

2009). In many global models (e.g., Neale et al. 2010), the entrainment rate is specified and is a parameter often adjusted to improve results; however, there are very few regional and global models in which the entrainment rate is empirically estimated (e.g., Kain 2004; Chikira and Sugiyama 2010; Del Genio et al. 2012). But for high-resolution simulations, assumptions made in the entrainment formulation of the KF scheme need to be reconsidered. The convective momentum transport by cumulus convection is not included in many regional models, but for high-resolution modeling the importance of including such subgrid-scale transport on grid-scale vertical motions deserves attention since it could help reduce model spinup time.

Based on the above considerations, a few updates that were explored using the KF convective scheme are the following: inclusion of subgrid-scale cloud radiation interactions, a dynamic adjustment time scale, impact of subgrid-scale cloud updraft mass fluxes on grid-scale vertical velocity, and an entrainment methodology based on the lifting condensation level (LCL). These changes introduce scale dependency for some of these key parameters in the KF scheme with an expectation that they will improve weather forecasts at 9- and 3-km grid spacings.

Since forecasts are sensitive to the initial conditions and small changes in the initial conditions can lead to big changes farther out in time (Rabier et al. 1996; Stensrud et al. 2000), an accurate specification of the initial model state (i.e., the analysis of the atmospheric state) can make a significant improvement in high-resolution NWP model forecasts (Ehrendorfer 1997; Simmons and Hollingsworth 2002). In this study, we also explore impacts of initial conditions on short-term high-resolution forecasts, as well as the sensitivity to different initial conditions of a high-resolution NWP model that includes an updated parameterized cloud dynamics. For that reason, we have made an attempt to study the impacts of introducing scale-aware convective parameterized cloud dynamics for high-resolution forecasts using two different initial analyses.

To improve the prediction of precipitation distribution and variability, this study introduces several changes to the KF convective parameterization scheme in the WRF Model and evaluates their impacts on high-resolution short-term forecasts. Since high-resolution models can have varying degrees of sensitivities to physics, dynamics, and initial conditions, the objectives of this study are limited to understanding of the impacts of using 1) initial conditions obtained from two different analysis fields, and 2) a scale-dependent updated KF scheme on high-resolution precipitation forecasts using WRF, version 3.4.1 (Skamarock and Klemp 2008). This paper is organized as follows: section 2 presents methods for updating the KF scheme, section 3 describes the design of the numerical simulations, section 4 evaluates the WRF Model performance, and the summary and conclusions are provided in section 5.

2. Methodology

For the purpose of improving high-resolution precipitation forecasts, we developed an updated KF scheme based on the study of subgrid-scale cloud–radiation interactions by Alapaty et al. (2012) by introducing grid resolution dependency and modifying the adjustment time scale and entrainment processes that influence surface precipitation. To help mitigate model spinup issues in short-range weather forecasts and associated precipitation, we also considered the impacts of subgrid-scale cloud updraft mass fluxes on grid-scale vertical velocity.

Multisensor precipitation estimates (MPE; also known as stage-IV next-generation radar), hourly rainfall products, and the satellite infrared cloud observations were used for validation of the model forecasts. MPE stage IV is a national precipitation analysis obtained from consideration of next-generation radar data and precipitation gauges (Lin and Mitchell 2005). MPE data at 4-km spatial resolution were obtained at hourly intervals and interpolated for a 3-km grid spacing in our study. The high spatial resolution of MPE data makes it possible to evaluate high-resolution NWP model precipitation forecasts.

a. The KF convective parameterization scheme

The KF convective parameterization scheme (Kain and Fritsch 1990, 1993; Kain 2004) has been used successfully over the years, incorporated in the fifth-generation Pennsylvania State University–National Center for Atmospheric Research Mesoscale Model (MM5; Wang and Seaman 1997), the National Centers for Environmental Prediction (NCEP) Eta Model (Black 1994), the WRF Model (Skamarock and Klemp 2008), and the new Model for Prediction Across Scales (MPAS; Skamarock et al. 2012). The KF scheme is a mass flux parameterization and uses the Lagrangian parcel method, and it can be generally grouped into three parts: 1) the convective trigger function, 2) the mass flux formulation, and 3) the closure assumptions. The early version of the KF scheme (Kain and Fritsch 1990, 1993) utilized a simple cloud model with moist updrafts and downdrafts, and has been modified for use by NWP models. Several components of that KF scheme have been changed (Kain 2004) to include an updraft formulation (i.e., imposing a minimum entrainment

rate, specified cloud radius to vary as a function of subcloud-layer convergence, allowing a minimum cloud depth to vary as a function of cloud-base temperature, and allowing shallow convection), a downdraft formulation (i.e., introducing a new downdraft algorithm), and a closure assumption (i.e., calculating CAPE based on the path of an entraining parcel). In this study, we have used that latest version of the KF scheme (i.e., Kain 2004) to introduce several new science updates that are described in the following section.

b. *A brief description of subgrid-scale cloud–radiation interactions*

In most NWP models, subgrid-scale convective parameterizations do not consider cumulus cloud feedbacks to radiation due to a lack of knowledge on how to estimate fractional cloudiness as a function of parameterized clouds, resulting in biases in both regional weather and climate simulations (Herwehe et al. 2014). Alapaty et al. (2012) introduced a subgrid-scale cumulus cloudiness formulation to the KF convective parameterization scheme (Kain 2004) and the RRTMG model (Iacono et al. 2008). The inclusion of subgrid-scale cloud–radiation interactions created more realistic longwave and shortwave radiation variability, leading to the improvement of several meteorological parameters at both the weather and climate time scales. Here, we extend the study of subgrid-scale cloud–radiation interactions by relaxing some of the assumptions used in the KF scheme and hypothesize that our updated KF scheme will reduce excessive precipitation in weather forecasts for short-term high-resolution modeling studies.

c. *A dynamic formulation for the adjustment time scale*

The adjustment time scale τ is the time over which CAPE is reduced to stabilize the atmosphere, originally introduced by Fritsch and Chappell (1980). In the default configuration of many NWP models, a constant value of τ is specified as a global constant. The KF scheme uses a technique that was proposed by Fritsch and Chappell (1980) for the estimation of τ based on the mean tropospheric horizontal wind speed and grid resolution. However, as noted by Stensrud (2007), this formulation may approach its limitation either for high-resolution grids or for environments with strong winds, such as hurricane simulations. Because of this limitation, τ was found to be one of the parameters that caused wet biases in simulated precipitation amounts at 12-km grid spacing (Bullock et al. 2015). As we move from coarser (~15 km) to high-resolution (~1 km) grids, one would expect the impacts of parameterized convection to gradually become less significant. However, many convective parameterization schemes cannot work properly at these finer scales because the tendencies produced by parameterized convection dominate over-resolved convection (Arakawa and Jung 2011; Molinari and Dudek 1992). To make convective parameterization schemes (such as KF) seamless across these spatial scales, τ should increase with increased grid resolution such that atmospheric stability restoration is gradually taken over by the resolved convective processes. However, it does not occur with the existing τ methodology used in the KF scheme as demonstrated by Bullock et al. (2015). To that effect, a formulation for τ is developed by using cloud macrophysical parameters following the notion used by Bechtold et al. (2008).

Considering the fact that many KF parameters are tied to grid spacing of around 25 km (Kain 2004), we derive a new grid resolution–dependent dynamic formulation of the adjustment time scale based on Bechtold et al. (2008):

$$\tau = \frac{\text{depth scale}}{\text{velocity scale}} F_n(Dx), \tag{1}$$

$$\tau = \frac{H}{W}\beta, \quad \text{and} \tag{2}$$

$$\beta = \left[1 + \ln\left(\frac{25}{Dx}\right)\right], \tag{3}$$

where H is cloud depth (m), W is cloud-averaged vertical velocity (m s^{-1}), Dx is the horizontal grid spacing (km), and β is a scaling parameter dependent on the model's horizontal grid spacing Dx (km), analogous to but different from that of Bechtold et al. (2008).

For a spectrum of grid resolutions, the adjustment time scale τ from Eq. (1) without the scaling parameter β would be of the same order. Thus, as argued earlier, the scaling parameter helps the scheme represent a smooth transition from parameterized cloud physics to resolved grid-scale cloud physics. For a 25-km grid, the scaling parameter β will become 1.0, while for a 1-km grid it would be about 4 times larger. Proposed spatial variation of the scaling parameter closely follows the logarithmic-bimodal distribution of cloud fraction dependency on horizontal grid resolution derived from a cloud-resolving modeling study (Arakawa and Wu 2013). In our study, as resolution increases, τ increases and thus reduces the number of parameterized updrafts, which conforms to the main theme of Arakawa and Wu (2013) that subgrid-scale cloud fraction should cover only a small portion of a grid cell. Since the cloud depth H is readily available from the KF, cloud-averaged vertical velocity scale W is the only unknown in Eq. (2) and it is estimated as follows.

We extend the shallow convection study of Grant and Lock (2004) that used large-eddy simulations (LES) and observations of the Barbados Oceanographic and Meteorological Experiment (BOMEX; Holland and Rasmusson 1973) to relate cloud depth-averaged vertical velocity W to the product of KF cloud-base updraft mass flux and entrained CAPE as

$$W = (\delta m_b A_e)^{1/3}, \tag{4}$$

where δ is a constant and set to unity so that Eq. (4) is consistent with that of Grant and Lock, m_b is the cloud-base updraft mass flux per unit density ($\mathrm{m\,s^{-1}}$), and A_e is diluted/entrained CAPE ($\mathrm{m^2\,s^{-2}}$).

Since Eq. (4) was originally developed for shallow convective clouds, in order to extend it for deep convective clouds, we have introduced the constant δ. It is interesting to note that Grant and Lock (2004) did not note that Eq. (4) is related to the cloud work function originally proposed by Arakawa and Schubert (1974) for a spectrum of convective clouds. Thus, Eq. (4) also works for deep convective clouds since it is essentially the cubed root of a simplified form of the cloud work function. The cloud work function is defined as the buoyancy flux contribution to the rate of change of convective kinetic energy per unit of cloud-base mass flux, which then can be related to the product of vertically averaged cloud mass flux and entrained CAPE (A_e). Thus, δ becomes the ratio of vertically averaged cloud mass flux and cloud-base mass flux, resulting in Eq. (4). From the study of Lawrence and Rasch (2005) that used the Zhang and McFarlane (1995) scheme, we find that vertically averaged mass flux is very close to the cloud-base mass flux and thus δ can vary from about 0.9 to 1.1 for deep convection. However, in this study, we set δ to unity for the deep moist convection.

Our new dynamic formulation for the adjustment time scale can then be written as

$$\tau = \frac{H}{(\delta m_b A_e)^{1/3}}\beta = \frac{H}{(\delta m_b A_e)^{1/3}}\left[1 + \ln\left(\frac{25}{Dx}\right)\right]. \tag{5}$$

Thus, the adjustment time scale in Eq. (5) increases as resolution increases, resulting in longer time allowed for CAPE consumption by parameterized cloud physics and, hence, stabilization of the atmosphere by the KF scheme, facilitating a gradual transition of the stability restoration by the KF scheme to the grid-scale cloud physics.

d. *Enhancement of grid-scale vertical velocity using subgrid-scale updraft mass fluxes*

Many studies (e.g., Han and Pan 2011; Richter and Rasch 2008; Mallard et al. 2013) cite the need for inclusion of convective momentum transport into the KF scheme for proper simulation of hurricanes. But, for high-resolution convective precipitation forecasts, it is not clear whether subgrid-scale updraft mass flux plays an important role on grid-scale momentum, mass, and energy transport. To address an aspect of this issue, we considered impacts of subgrid-scale updraft mass fluxes on grid-scale vertical velocity using a simple linear methodology. One potential benefit is that it can help reduce model spinup time over convectively active regions by increasing the grid-scale vertical velocity. The proposed simple linear mixing methodology for enhancing grid-scale vertical velocity is expressed as

$$W_{\mathrm{up}} = \frac{M_{\mathrm{up}}}{\rho} = \frac{M/Dx^2}{\rho}, \quad \text{and} \tag{6}$$

$$W_n = W_g + W_{\mathrm{up}}, \tag{7}$$

where W_{up} is the effective vertical velocity of subgrid-scale updraft ($\mathrm{m\,s^{-1}}$), M_{up} is the subgrid-scale updraft mass flux ($\mathrm{kg\,m^{-2}\,s^{-1}}$), ρ is the convective plume density ($\mathrm{kg\,m^{-3}}$), M is the updraft mass rate ($\mathrm{kg\,s^{-1}}$), W_n is the reformulated grid-scale vertical velocity ($\mathrm{m\,s^{-1}}$), and W_g is the grid-scale vertical velocity ($\mathrm{m\,s^{-1}}$).

e. *Entrainment methodology based on LCL*

From Kain (2004) the equation of the minimum entrainment rate for convective plumes is given by

$$\Delta M_e = M_b \frac{C}{R}\Delta P, \tag{8}$$

where ΔM_e is the mixing rate ($\mathrm{kg\,s^{-1}}$); M_b is the updraft mass rate at cloud base ($\mathrm{kg\,s^{-1}}$); $C = 0.03$ is a constant ($\mathrm{m\,Pa^{-1}}$), which controls the overall magnitude of the entrainment rate for convective plumes; R is the radius of cloud base and dependent on the magnitude of vertical velocity at the LCL (m); and ΔP is the pressure depth of a model layer (Pa).

The magnitude of the constant C used in the Eq. (8) is the same as that of the nondimensional Tokioka parameter, $\alpha = 0.03$ (Tokioka et al. 1988), used in global climate studies (e.g., Kang et al. 2009; Kim et al. 2011; Lin et al. 2013) for entrainment rate estimation. These global studies showed that the hyperactivity of a subgrid-scale convection scheme can be largely modulated by tuning the Tokioka parameter, which allows grid-scale processes to perform the needed moisture conditioning of the large-scale atmosphere. These studies also showed that the subgrid-scale precipitation decreases as the Tokioka parameter increases, resulting in an increase of grid-scale precipitation for improved climate simulations. Dependence of the entrainment on

TABLE 1. Summary of the numerical experiments.

Simulation period	Expt No.	Expt name	Initial conditions	Microphysics scheme	9-km grid spacing	3-km grid spacing
0000 UTC 4 Jun–0000 UTC 6 Jun 2002	1	EXP	GFS	Goddard microphysics scheme	KF scheme	No cumulus parameterization
	2		CFSR			
	3	BASE	GFS		KF scheme	KF scheme
	4		CFSR			
	5	UKF	GFS		Updated KF scheme	Updated KF scheme
	6		CFSR			
0600 UTC 16 Jun–0600 UTC 18 Jun 2002	7	EXP	GFS	Goddard microphysics scheme	KF scheme	No cumulus parameterization
	8		CFSR			
	9	BASE	GFS		KF scheme	KF scheme
	10		CFSR			
	11	UKF	GFS		Updated KF scheme	Updated KF scheme
	12		CFSR			
0000 UTC 5 Jul–0000 UTC 7 Jul 2010	13	EXP	GFS	Goddard microphysics scheme	KF scheme	No cumulus parameterization
	14		CFSR			
	15	BASE	GFS		KF scheme	KF scheme
	16		CFSR			
	17	UKF	GFS		Updated KF scheme	Updated KF scheme
	18		CFSR			
0000 UTC 28 Jul–0000 UTC 30 Jul 2010	19	EXP	GFS	Goddard microphysics scheme	KF scheme	No cumulus parameterization
	20		CFSR			
	21	BASE	GFS		KF scheme	KF scheme
	22		CFSR			
	23	UKF	GFS		Updated KF scheme	Updated KF scheme
	24		CFSR			
	25	DYNTAU	GFS		KF scheme with only dynamic τ update	
	26		CFSR			
	27	WUP	GFS		KF scheme with only updraft mass flux update	
	28		CFSR			
	29	ENT	GFS		KF scheme with only entrainment update	
	30		CFSR			
0600 UTC 16 Jun–0600 UTC 18 Jun 2002	31	EXP	GFS	WDM6 scheme	KF scheme	No cumulus parameterization
	32		CFSR			
	33	BASE	GFS		KF scheme	KF scheme
	34		CFSR			
	35	UKF	GFS		Updated KF scheme	Updated KF scheme
	36		CFSR			

horizontal grid resolution for radiatively driven shallow (stratocumulus) clouds was studied by Stevens and Bretherton (1999) using a large-eddy simulation model. Their study found that when the horizontal spacing is coarsened, the entrainment rate decreased without any noticeable changes in the overall structure of the subcloud layer and cloud layer. The role of entrainment for continental deep convective clouds was extensively studied by Del Genio and Wu (2010). One of their findings was that at finer spatial resolutions, their inferred entrainment rate was greater because turbulence was more resolved. They also used the WRF Model at different grid resolutions and found the inferred entrainment rate at 125-m grid spacing to be stronger than that inferred at 600-m grid spacing. Entrainment in deep convective clouds was also studied by Romps and Kuang (2010) using a LES model. It was shown that the purity of convection decreases with finer grids (ranging from 3200- to 100-m spacings), suggesting increased entrainment with finer grid spacing. Finally, in a recent cloud resolving modeling study, Bryan and Morrison (2012) concluded that changes in the simulated squall-line intensity differences between two model grid resolutions (1- and 0.25-km grid spacing) were primarily attributed to the increased entrainment. Thus, all these studies clearly highlighted the dependency of entrainment on the horizontal grid resolution (i.e., entrainment increases as grid resolution increases). de Rooy et al. (2013) provide a detailed review of entrainment in cumulus convection and highlights the study of Houghton and Cramer (1951) that entrainment needs to be partitioned into two parts: 1) entrainment due to large-scale processes and 2) entrainment due to turbulence at cloud edges. Since the first type of entrainment is being

represented by Eq. (8), we have included the second type of entrainment through the usage of the Tokioka parameter. Thus, we considered all of these findings when reformulating the entrainment rate [Eq. (8)] in the KF scheme to make it more adaptable to high-resolution model forecasts and to work seamlessly across spatial scales. We introduce this feature via a dynamic Tokioka parameter that increases as model resolution increases. Thus, the resolution-dependent Tokioka parameter helps to represent grid spacing effects on convective cloud–entrainment interactions similar to that documented in the literature. Hence, consistent with the above global climate and large-eddy simulation studies, we have introduced a scale dependency for the Tokioka parameter by multiplying it with the β shown in Eq. (3), and also replaced R by Z_{LCL} (m)—subcloud layer depth—which is the height of the LCL above the ground. The main advantage of using Z_{LCL} instead of R is that at higher resolutions, R generally approaches the upper limit of 2 km used in the KF scheme, thus, it is not consistent with the assumption that subgrid-scale cloud fraction covers only a small area of a grid cell (e.g., Arakawa and Wu 2013). In such situations, the diameter of the KF cloud will become 4 km and thus, at the 3-km grid spacing used in this study, usage of R is inappropriate as the assumed subgrid cloud diameter exceeds the grid size.

Then, the new minimum entrainment equation can be written as

$$\Delta M_e = M_b \frac{\alpha\beta}{Z_{\mathrm{LCL}}} \Delta P. \tag{9}$$

Thus, Eq. (9) attempts to include both the types of entrainment consistent with the descriptions of de Rooy et al. (2013).

3. Design of simulations

The WRF Model (Skamarock and Klemp 2008) is commonly used for a wide range of meteorological studies across scales ranging from meters to thousands of kilometers and time scales from days to decades. An increasing number of researchers are employing it to study regional weather (e.g., Chen et al. 2011) and historic and future climate (e.g., Otte et al. 2012). However, recent regional climate research noted that WRF often produced excessive precipitation within highly energetic convective systems (Done et al. 2004; Hong et al. 2010; Alapaty et al. 2012; Herwehe et al. 2014). We hypothesize that including the effects of parameterized scale-aware cloud dynamics into a high-resolution WRF simulation will reduce the excessive rainfall biases by properly representing convective time scale, grid-scale vertical velocity, and entrainment effects.

The WRF Model, version 3.4.1, was used to conduct all weather forecast simulations over the U.S. southern Great Plains (SGP) due to its importance as a

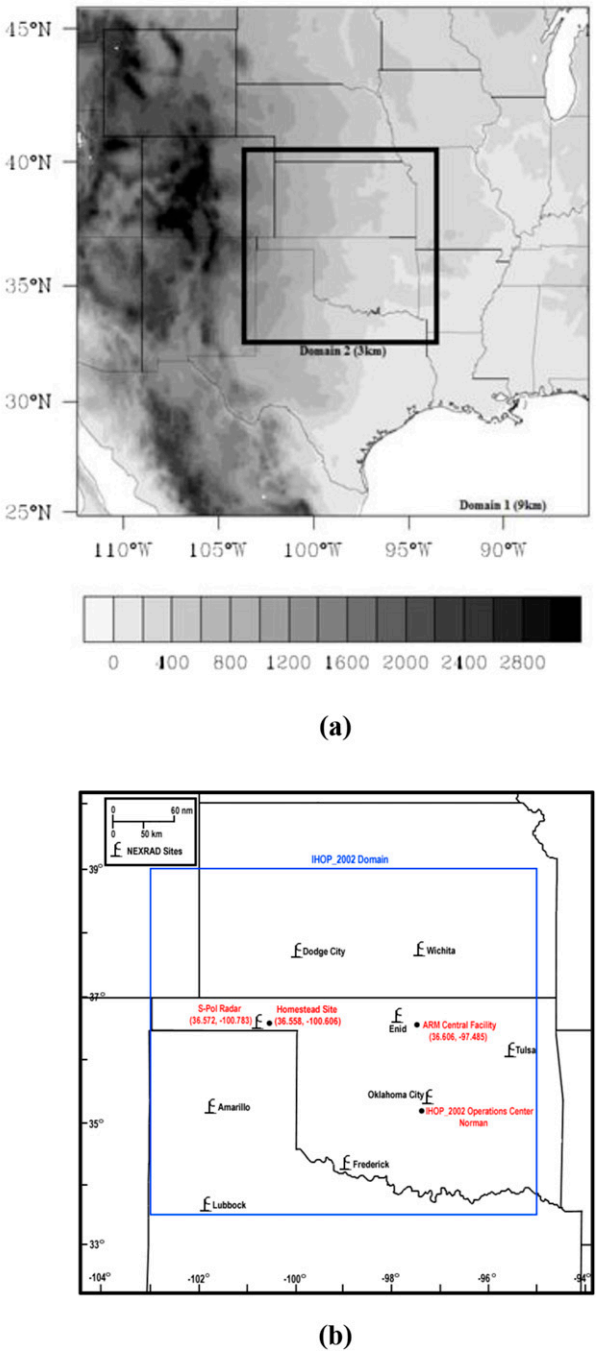

FIG. 1. (a) Topographic map of the nested model domain over the U.S. southern Great Plains (SGP) and (b) the IHOP_2002 domain and fixed deployment locations (https://www.eol.ucar.edu/field_projects/ihop2002).

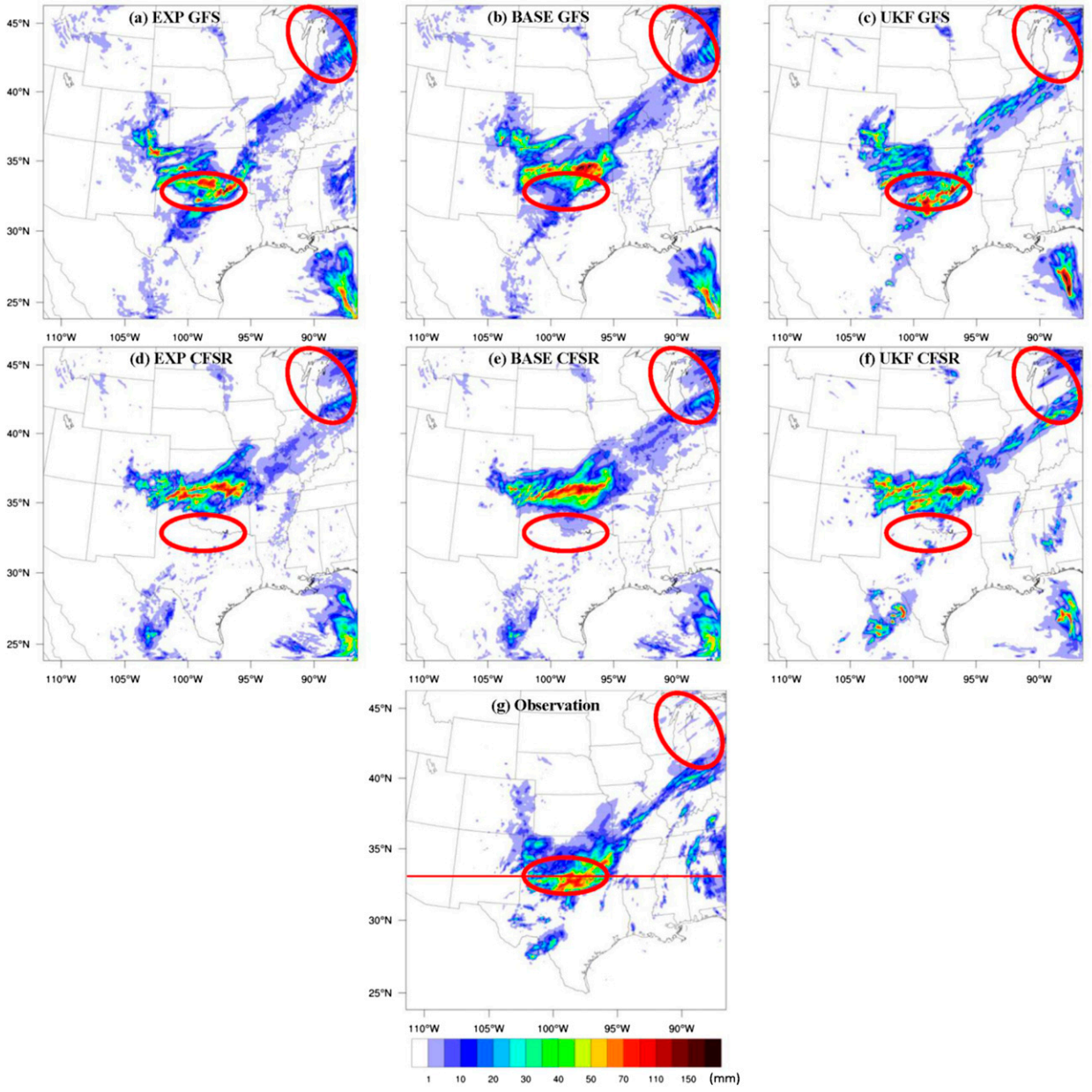

FIG. 2. Comparative example of simulated 12-h (0000–1200 UTC 5 Jun 2002) accumulated precipitation (mm) over a 9-km grid spacing domain with (top) GFS and (middle) CFSR for (a),(d) EXP; (b),(e) BASE; (c),(f) UKF; and (g) stage-IV observed precipitation.

land–atmosphere coupling "hotspot" (Koster et al. 2004; Zheng et al. 2015) and the availability of various observations. The main land-cover types include grassland, cropland, savannas, and a mixture of crop and natural vegetation (Holt et al. 2006; LeMone et al. 2007).

To understand the effects of using parameterized cloud dynamics for high-resolution forecasts, we tested three WRF Model configurations with two-way interacting nests for the SGP. In our model simulations we used two choices [the Goddard microphysics scheme and the WRF double-moment 6-class scheme (WDM6)] for grid-scale cloud processes for both grid spacings (9 and 3 km). However, for subgrid-scale cloud representation, we used three approaches: 1) disabled subgrid-scale convection, allowing only explicit convection; 2) the latest KF scheme (Kain 2004); and 3) our updated KF scheme. Details on the cloud formulations used in this study are described in Table 1, showing a total of 36 numerical experiments. We have assigned a unique experiment name for each set of numerical simulations and

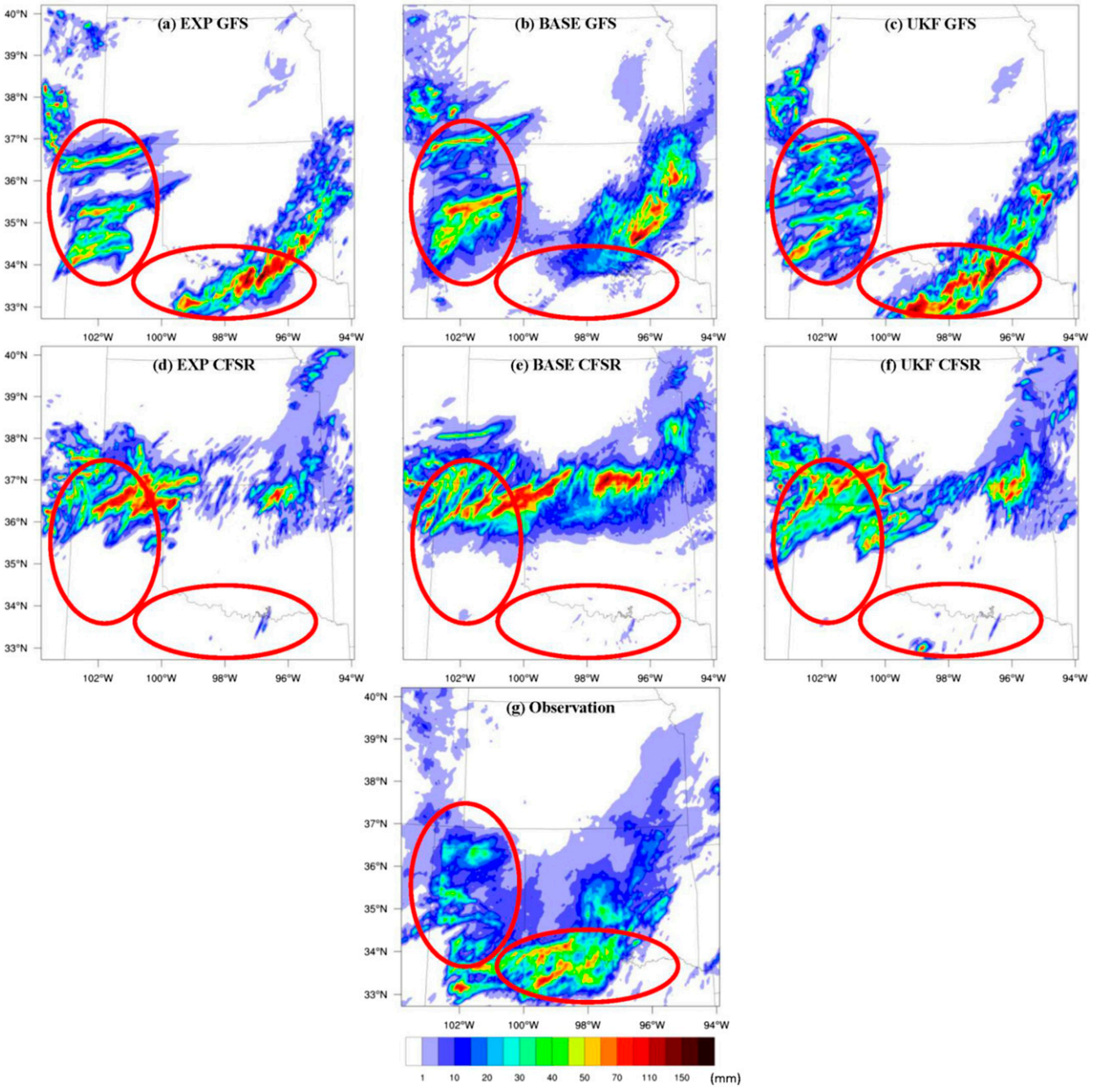

FIG. 3. Comparative example of simulated 6-h (0000–0600 UTC 5 Jun 2002) accumulated precipitation (mm) over a 3-km grid spacing domain with (top) GFS and (middle) CFSR for (a),(d) EXP; (b),(e) BASE; (c),(f) UKF; and (g) stage-IV observed precipitation.

these are referred to as EXP (explicit convection only), BASE [with the Kain (2004) KF], and UKF (with the updated KF). For example, for each simulation period, the EXP case has two numerical simulations, as identified under experiment number in Table 1, referring to two types of initial conditions. To study impacts due to the choice of microphysics representation with the updated KF scheme and its effects on regional weather simulations, we performed another set of six numerical experiments. These experiments were designed to compare the performance of the Goddard microphysics scheme with the WDM6. Note that no nudging or data assimilation was used in any of the simulations.

The 1° 6-hourly NCEP Global Final Analysis (FNL) data derived from the Global Forecast System (GFS) and 0.5° 6-hourly Climate Forecast System Reanalysis (CFSR) data were used separately to develop lateral boundary and initial conditions for the large-scale atmospheric fields, soil parameters (i.e., soil moisture and temperature), and sea surface temperature (SST). The WRF Model was

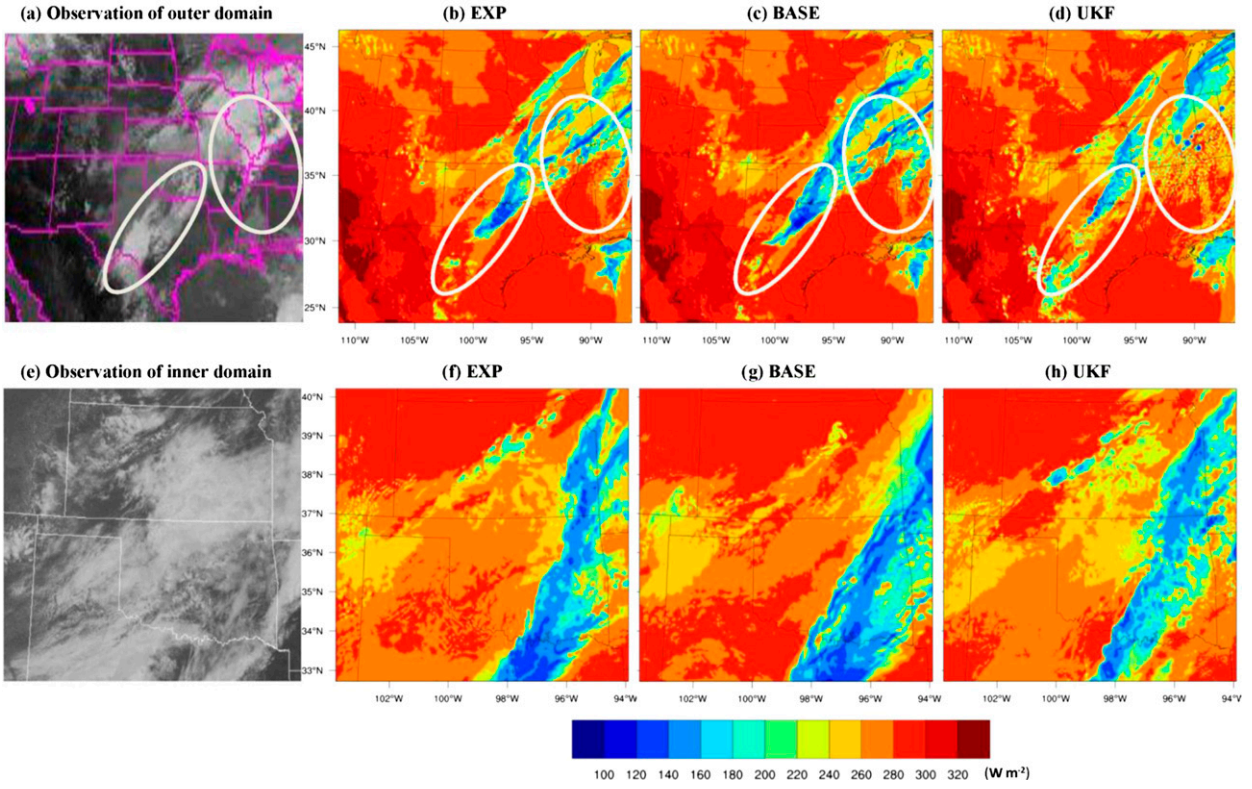

FIG. 4. Outgoing longwave radiation (W m^{-2}) with GFS at 1800 UTC (1300 CDT) 5 Jun 2002 over (top) a 9-km grid spacing domain and (bottom) a 3-km grid spacing domain for (b),(f) EXP; (c),(g) BASE; and (d),(h) UKF.

configured with two-way interactive nested domains using horizontal grid spacing of 9 km (290 × 280 grid points; domain 1 in Fig. 1a) and 3 km (307 × 274 grid points; domain 2 in Fig. 1a). Locations of observational sites in domain 2 are shown in Fig. 1b. In the vertical, the model was configured with 28 eta levels with a model top at 50 hPa. Prominent physics options in the WRF Model configuration included the RRTMG radiation models (Iacono et al. 2008), the Goddard microphysics scheme (Tao et al. 1989), the Mellor–Yamada–Janjić (MYJ) planetary boundary layer (PBL) scheme (Janjić 2002), and the Noah land surface model (Chen and Dudhia 2001). We focus our evaluation on assessing the updated model's ability to forecast the location and intensity of surface precipitation, surface longwave and shortwave radiation, and surface temperature fields.

4. Results and discussion

The primary goal of this study is to investigate the suitability of the updated KF scheme for high-resolution simulations representing and forecasting surface precipitation. Another goal is to study the impacts of two types of initial conditions obtained from different analyses on high-resolution model simulations. For this purpose, WRF simulations using the 1.0° 6-hourly FNL datasets derived from GFS (denoted as GFS) to specify the initial states as well as boundary conditions are compared to those which used the 0.5° 6-hourly CFSR data (denoted as CFSR) as initial and boundary conditions. Four different regional precipitation patterns and time periods were selected for this experiment. An additional microphysics scheme sensitivity study (using the Goddard and WDM6 microphysics schemes) was designed to explore whether various microphysics schemes accompanied with the updated KF scheme are able to produce appropriate precipitation forecasts for these high-resolution simulations.

a. Simulation period 0000 UTC 4 June–0000 UTC 6 June 2002: Experiments 1–6

Representative examples of observed and simulated 12-h accumulated precipitation at 9-km grid spacing and 6-h accumulated precipitation at 3-km grid spacing starting at 0000 UTC 5 June 2002 are shown in Figs. 2 and 3. It is apparent that the model forecasts with GFS contain precipitation at appropriate general locations and with a similar spatial structure when compared to the stage-IV observed precipitation (Figs. 2g and 3g). However, the precipitation forecasts over the central to

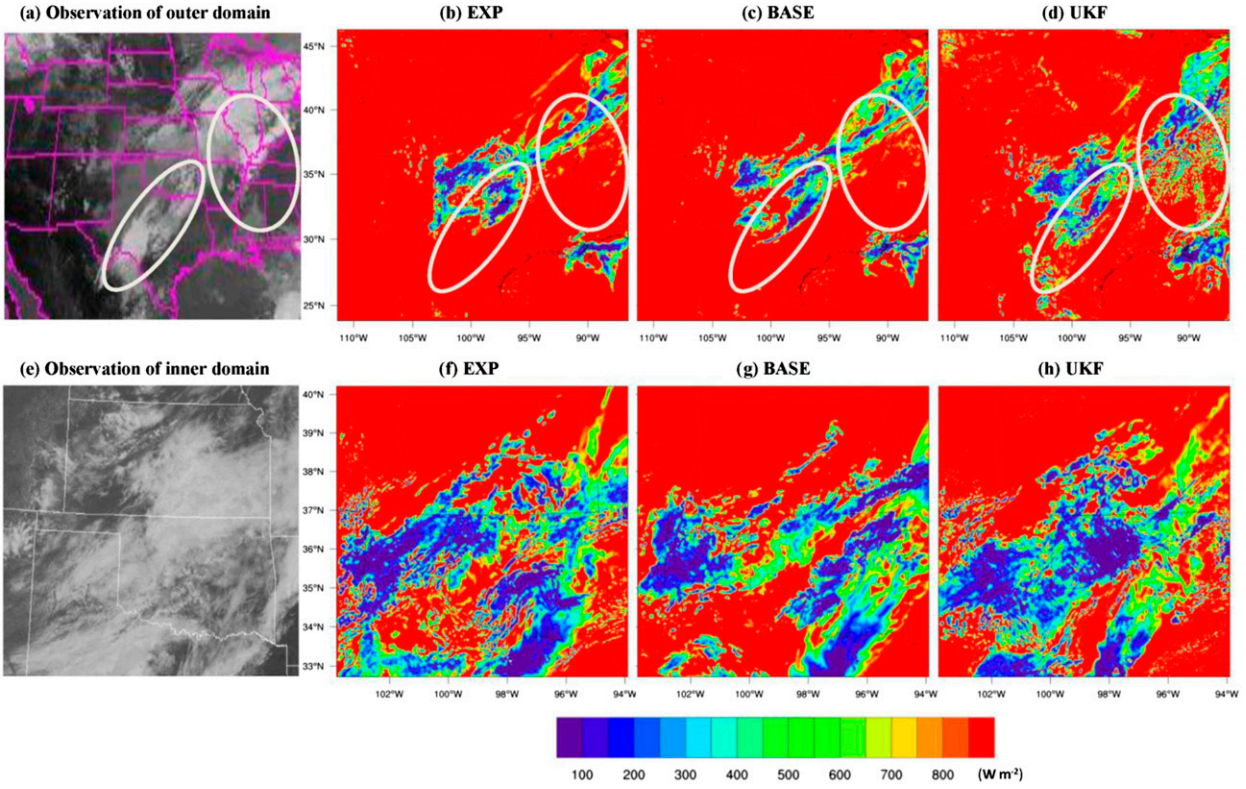

FIG. 5. Surface shortwave radiation ($W\,m^{-2}$) with GFS at 1800 UTC (1300 CDT) 5 Jun 2002 over (top) a 9-km grid spacing domain and (bottom) a 3-km grid spacing domain for (b),(f) EXP; (c),(g) BASE; and (d),(h) UKF.

eastern regions of the domains using CFSR as initial and boundary conditions (Figs. 2d–f and Figs. 3d–f) are shifted to the north, while in Figs. 2d–f the precipitation patterns over central Mexico and the Gulf of Mexico (based on observed cloud cover) seem to be reasonably simulated. Such precipitation location offset indicates that the reanalysis systems may be impacted by interactions between the observational data and the assimilation system and can create unrealistic precipitation distributions shortly after the model is initialized. It also indicates that some forecasts are more sensitive to initialization than to convective parameterization or physics. The 6-h accumulated precipitation from the 3-km grid spacing UKF GFS forecast (Fig. 3c) depicts a broad area of heavy precipitation over the western parts of the domain similar to that seen in the observations (Fig. 3g). It is also noted that the high-resolution UKF model simulations show improvement in the precipitation distribution. For instance, in Figs. 2 and 3 the heavy precipitation that occurred along the border of Oklahoma and Texas is shifted to the north and east in the BASE run (Figs. 2b and 3b), but is well simulated by the UKF run (Figs. 2c and 3c). In addition, around Lake Michigan the 12-h accumulated precipitation from the 9-km grid spacing forecast from UKF (Fig. 2c) has less coverage than that in the other two model runs using EXP and BASE (Figs. 2a and 2b), again making UKF's precipitation coverage more similar to the observations. Note that the MPE observations are only limited to land areas and thus no observational data exists over the ocean. Thus, large precipitation over the ocean (bottom-right corner in the Figs. 2a–f) simulated by the model cannot be verified.

For cloudy skies, outgoing longwave radiation (OLR) is reduced as opposed to clear skies and thus intercomparison of modeled OLR ($W\,m^{-2}$) can point out differences in simulations of cloud placement and depth. The OLR at 1800 UTC (1300 CDT) 5 June 2002 for WRF simulations with GFS for the 9- and 3-km grid spacing domains (experiments 1, 3, and 5 in Table 1) are shown in Fig. 4. The time shown is for the 42nd forecast hour of the 48-h simulations when convection is active. Satellite cloud coverage images available from NOAA's Aviation Digital Data Services (http://aviationweather.gov/adds/) are used for comparison to the EXP, BASE, and UKF runs. The OLR over the 9-km grid spacing domain (Figs. 4a–d) indicates that the southwest–northeast orientation of a band of low OLR for the UKF is more comparable to the satellite observation and contains more detailed information due to the subgrid-scale effects that are included here but not present in the BASE and EXP runs. It also shows less OLR

for the UKF due to subgrid clouds (i.e., Michigan, Alabama, Mississippi, and Texas) and more OLR under less cloudy regions (i.e., Indiana, Ohio, and Kentucky) compared with those for EXP and BASE. In addition, as one of the key components of the surface energy budget, the representation of downward shortwave radiation (DSR) is also used for the comparison. Figure 5 shows DSR for 1800 UTC (1300 CDT) 5 June 2002 along with satellite cloud coverage showing widespread cloudiness throughout Texas, Oklahoma, Missouri, Tennessee, Kentucky, Indiana, and Illinois. The DSR for the 9-km grid spacing over Tennessee, Kentucky, Mississippi, and Alabama in EXP and BASE indicates clear-sky conditions (Figs. 5b and 5c). However, in UKF, the DSR indicates more cloud coverage (Fig. 5d) similar to that seen in the observations (Fig. 5a). Further, the DSR for the 3-km grid spacing simulations (Figs. 5f–h) indicate that the cloud coverage for UKF is larger and in better agreement with the observations (Fig. 5e). This result is primarily because of the updated KF where the radiative effects of subgrid-scale clouds can be realistically represented even in grid spacing smaller than 4 km. Thus, the UKF configuration improves the cloud cover simulation, producing more realistic simulated radiation that could contribute to a better precipitation forecast.

Improved representation of cloudiness also affects the temporal variations of surface radiation in UKF for high-resolution model forecasts. For example, the measured 48-h variations of downward longwave and shortwave fluxes and the corresponding simulations at New Salem (37.31°N, 98.94°W), Kansas (IHOP_2002 site 7), at 3-km grid spacing (Figs. 6a and 6b) indicate that UKF modulates the radiative impacts in the model, particularly during the second day of the forecast. Both the EXP and BASE show large biases in shortwave fluxes with more than 600 W m^{-2} overestimations in the second day. The UKF simulation decreases the downward shortwave flux while increasing the downward longwave flux with the help of improved representation of cloudiness (Figs. 6a and 6b), leading to an overall improvement in the temporal variability of the surface fluxes. The increased cloudiness from UKF also reduces the surface temperature (Fig. 6c) by about 5°C. The UKF also shows a better simulation than the others in terms of variability, especially for the last 6 h of the run. However, the impact on the 2-m specific humidity (Fig. 6d) is not significantly different among runs because it depends on several land surface parameters such as soil moisture.

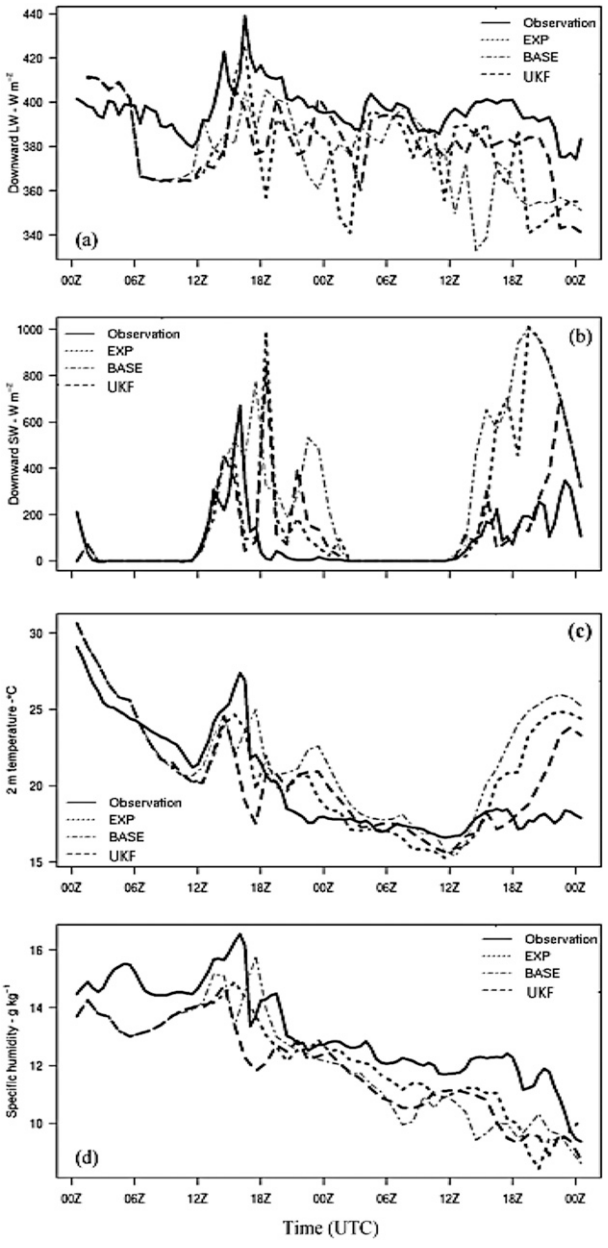

FIG. 6. The 48-h variation (0000 UTC 4 Jun–0000 UTC 6 Jun 2002) of (a) downward longwave flux at ground surface (W m^{-2}), (b) downward shortwave flux at ground surface (W m^{-2}), (c) temperature at 2 m (°C), and (d) specific humidity at 2 m (g kg^{-1}), at New Salem (37.31°N, 98.94°W), KS, from IHOP_2002 site 7 measurements (solid line) and corresponding simulations in EXP (dotted line), BASE (dot–dashed line), and UKF (dashed line) with GFS at 3-km grid spacing.

To study the functionality of the new science updates used in the KF scheme on the entire model atmosphere, we present sounding profiles (Fig. 7) at 0000 UTC 6 July 2002 for specific humidity, potential temperature, and wind speed at Norman, Oklahoma (OUN, 35.18°N, 97.44°W), and Topeka, Kansas (TOP, 39.07°N, 95.62°W), simulated at 3-km grid spacing and compared with respective observations available from the University of Wyoming (http://weather.uwyo.edu/upperair/sounding.html). For both observation sites, there is no clear

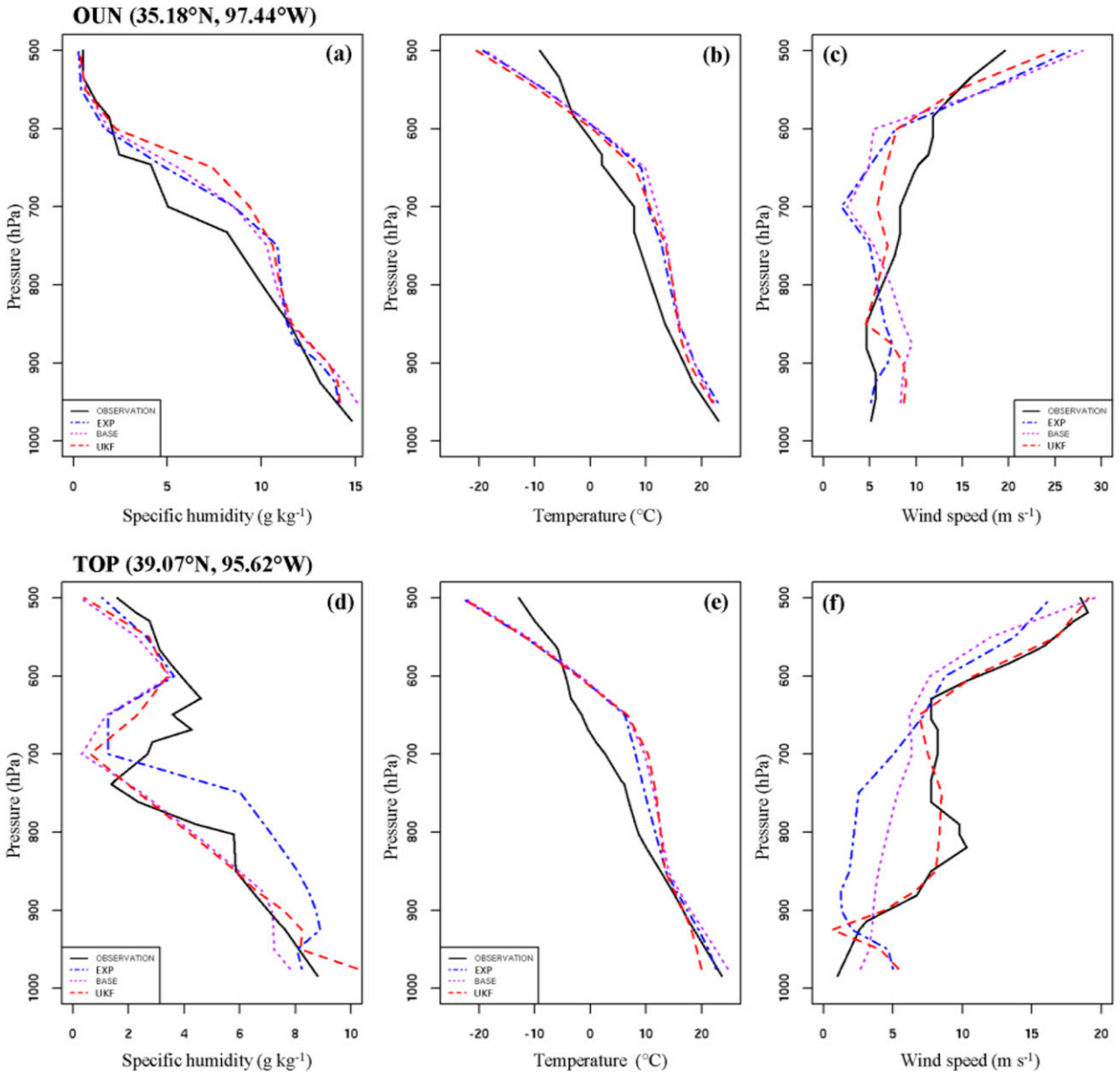

FIG. 7. Sounding profile at 0000 UTC 6 Jul 2002 of (a),(d) specific humidity (g kg^{-1}); (b),(e) potential temperature (K); and (c),(f) wind speed (m s^{-1}) valid at (top) Norman, OK (OUN, 35.18°N, 97.44°W), and (bottom) Topeka, KS (TOP, 39.07°N, 95.62°W).

indication of which simulation is outperforming the others, suggesting that the UKF has only minor differences with the other simulations for this observational time. However, tropospheric wind speeds and surface specific humidity simulated by the UKF seem to be closer to the observations. A detailed comparison of lower-tropospheric profiles is presented in the following section.

b. Simulation period 0000 UTC 28 July–0000 UTC 30 July 2010: Experiments 19–24

To extend this case study, a second set of 48-h simulations was initialized at 0000 UTC 28 July 2010 (experiments 19–24). Comparative examples of simulated 6-h accumulated precipitation on the second day over 9- and 3-km grid spacings are shown in Figs. 8 and 9. It is noted that the initial conditions still play an important role in the model simulation, but the precipitation forecast with CFSR has no spatial shift in this case, relative to observations. The general rainfall locations of UKF with GFS and CFSR are similar and close to the observations. The KF scheme in the EXP and the BASE runs with 9-km grid spacing again result in heavier amounts of rainfall (Figs. 8a,b and 8d,e), while UKF reduces the excessive precipitation and leads to a

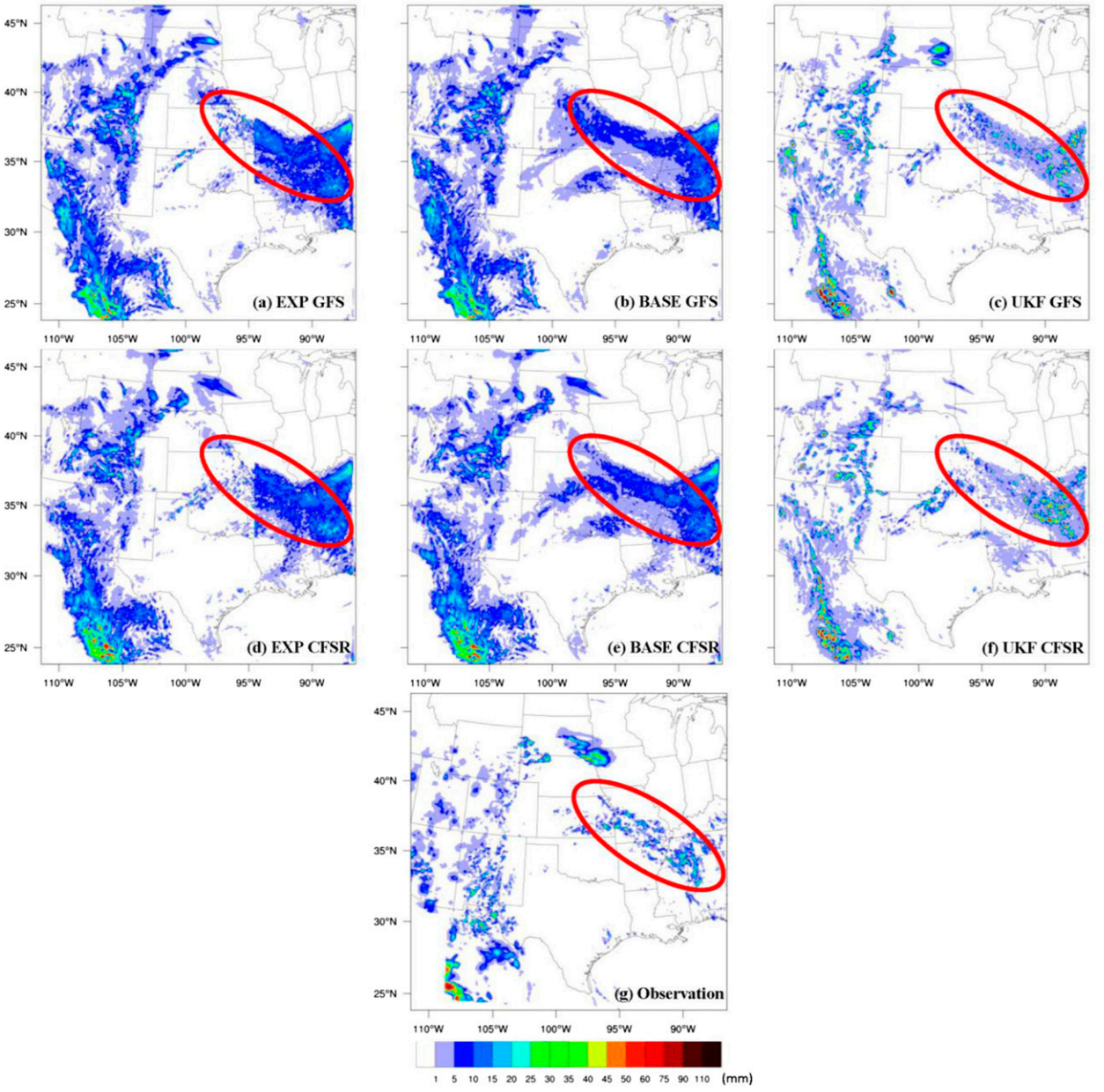

FIG. 8. Comparative example of simulated 6-h (1800 UTC 29 Jul–0000 UTC 30 Jul 2010) accumulated precipitation (mm) over a 9-km grid spacing domain with (top) GFS and (middle) CFSR for (a),(d) EXP; (b),(e) BASE; (c),(f) UKF; and (g) stage-IV observed precipitation.

much better simulation. In the 3-km grid spacing precipitation forecast (Fig. 9), excessive precipitation occurs with the BASE run, but better forecasts are evident in EXP and UKF. Since the high-resolution MPE (stage IV) hourly rainfall products have some biases (e.g., Wang et al. 2008; Westcott et al. 2008; Westcott 2009), the visible satellite cloud observation is included in the analysis to provide additional information. For the 9- and 3-km grid spacing runs, the observed 6-h accumulated precipitation does not exceed 1 mm in most of the northern Texas Panhandle, however, cloudiness (which is taken as a key input parameter in our research) can be seen in Texas in the visible satellite image (Fig. 9h). The observed cloudiness indicates that the precipitation fields simulated in the high-resolution grid by EXP and UKF in Figs. 9a, 9c, 9d, and 9f are comparable to each other. Furthermore, it is demonstrated that the explicit treatment of convection (no cumulus

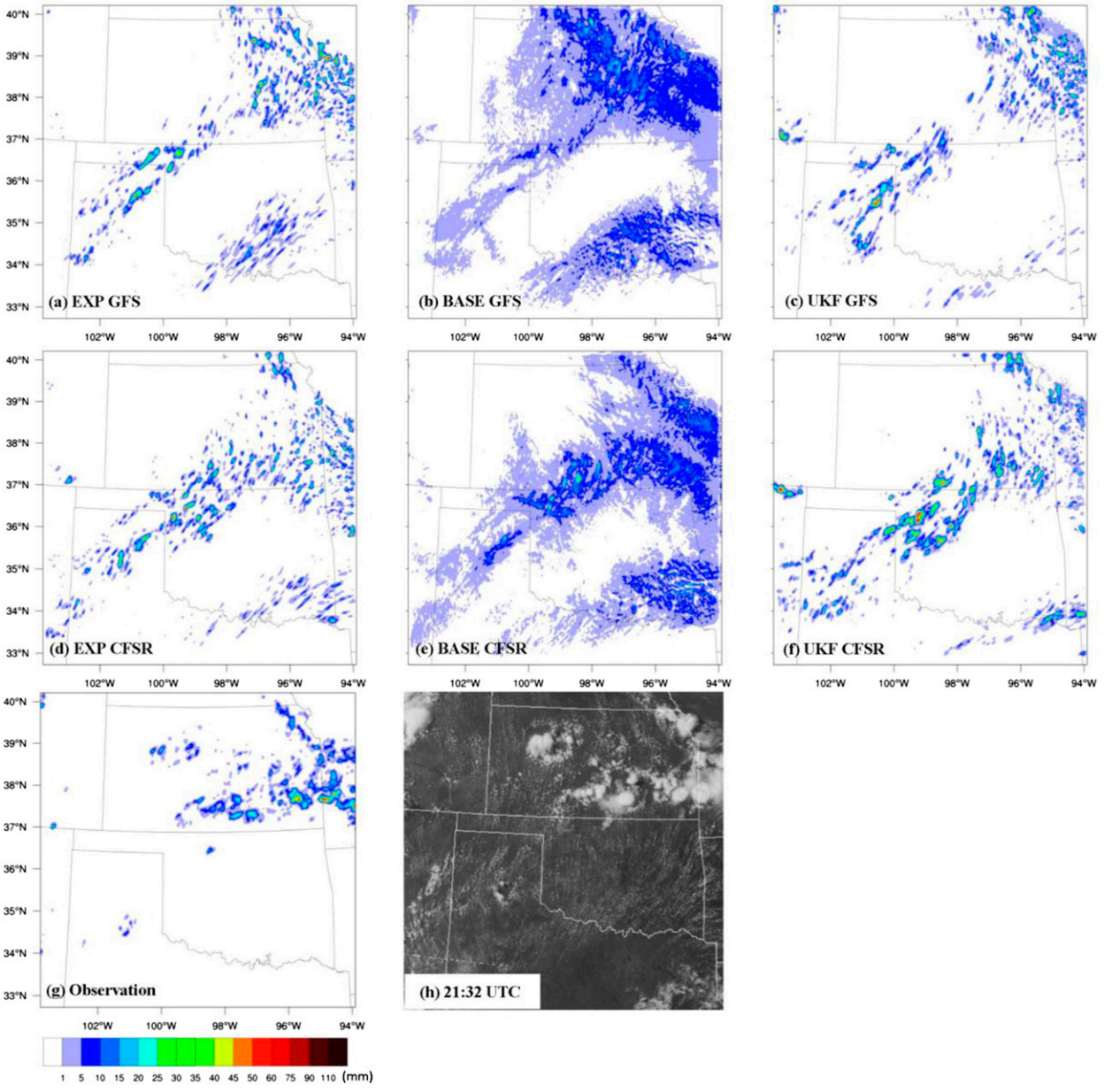

FIG. 9. Comparative example of simulated 6-h (1800 UTC 29 Jul–0000 UTC 30 Jul 2010) accumulated precipitation (mm) over a 3-km grid spacing domain with (top) GFS and (middle) CFSR for (a),(d) EXP; (b),(e) BASE; (c),(f) UKF; (g) stage-IV observed precipitation; and (h) visible satellite image valid at 2132 UTC 29 Jul 2010. The satellite image is obtained from http://aviationweather.gov/adds/ managed by NOAA's Aviation Digital Data Services.

parameterization) with a 3-km grid spacing at times can adequately predict convective systems and precipitation, consistent with the results of Done et al. (2004). For this case study, the UKF results successfully demonstrate that it does not decrease the accuracy of precipitation forecasts, relative to the EXP (explicit treatment of convection). However, Done et al. (2004) also pointed out that for some cases, explicit precipitation treatments suffered with an increasing propagated bias in the forecasts that may be mitigated by using the UKF treatment.

Three rain rate thresholds (5, 15, and 25 mm h^{-1}) were used to separate out light, medium, and heavy precipitation for the experiments. Within the thresholds, precipitation, which was accumulated over time, was area averaged over the 3-km grid spacing domain. Figure 10 shows the 48-h (0000 UTC 28 July–0000 UTC 30 July 2010) period area-averaged

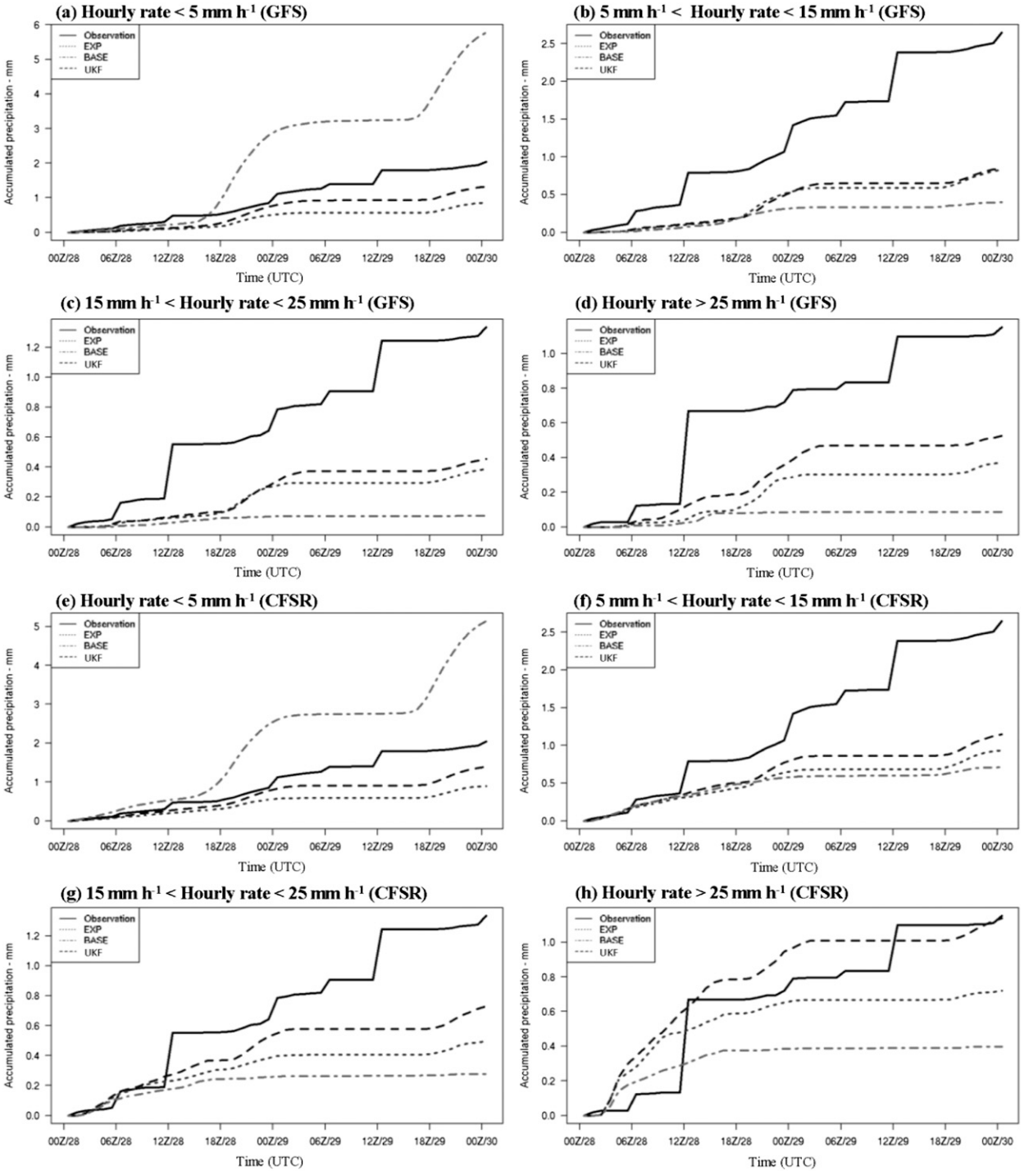

FIG. 10. The 48-h (0000 UTC 28 Jul–0000 UTC 30 Jul 2010) area averaged 3-km grid spacing precipitation (mm) from stage-IV observations (solid line) and corresponding simulations of EXP (dotted line), BASE (dot–dashed line), and UKF (dashed line) with (a)–(d) GFS and (e)–(h) CFSR.

accumulated precipitation for simulations in EXP, BASE, and UKF, reflecting dynamic changes in modeling of convective events, and for forecasts with GFS and CFSR, reflecting the change in initial and boundary conditions. As expected, results show that the area-averaged precipitation rates from the high-resolution simulation with UKF are closer to the corresponding stage-IV observations in precipitation intensity and the

TABLE 2. The 48-h averaged root-mean-square error (RMSE) of area-averaged precipitation rate over a 3-km grid spacing domain.

	GFS precipitation (mm h^{-1})				CFSR precipitation (mm h^{-1})			
	0–5	5–15	15–25	greater than 25	0–5	5–15	15–25	greater than 25
EXP	0.74	1.09	0.60	0.55	0.70	1.00	0.50	0.26
BASE	1.68	1.29	0.77	0.71	1.35	1.07	0.61	0.45
UKF	0.47	1.06	0.55	0.43	0.45	0.87	0.37	0.18

timing of convection initiation for both GFS and CFSR. It can be seen that improvements of the area-averaged precipitation are made by UKF with GFS for very light rain rates (0–5 mm h^{-1}), moderate rain rates (15–25 mm h^{-1}), and heavier rain rates (greater than 25 mm h^{-1}), while the BASE run performs poorest for all the rates. The difference in the light rain rates (5–15 mm h^{-1}) with GFS between EXP and UKF is very small. The area-averaged rainfall simulated using CFSR is found to be heavier compared to the GFS results. In addition, the 48-h averaged root-mean-square error (RMSE) for the 3-km domain is shown in Table 2. In general, the 48-h averaged RMSE of the area-averaged precipitation is greatly decreased by UKF for all rainfall rates. It indicates that UKF outperforms the other two simulations at every threshold, regardless of the dataset used for initial and boundary conditions. The differences in the area-averaged RMSE between GFS and CFSR for EXP are small (less than or equal to 0.10 mm h^{-1} at every threshold) for all but greater than 25 mm h^{-1} cases, while the differences for BASE are obviously larger (~0.16–0.33 mm h^{-1}). Although a negligibly small difference is seen for UKF for the very light rain rate, the differences in RMSE between GFS and CFSR for the other rates are larger. In the heavier rainfall threshold, differences in the 48-h averaged RMSE are significant for all the experiments (i.e., 0.29 mm h^{-1} for EXP, 0.26 mm h^{-1} for BASE, and 0.25 mm h^{-1} for UKF). These differences reflect the

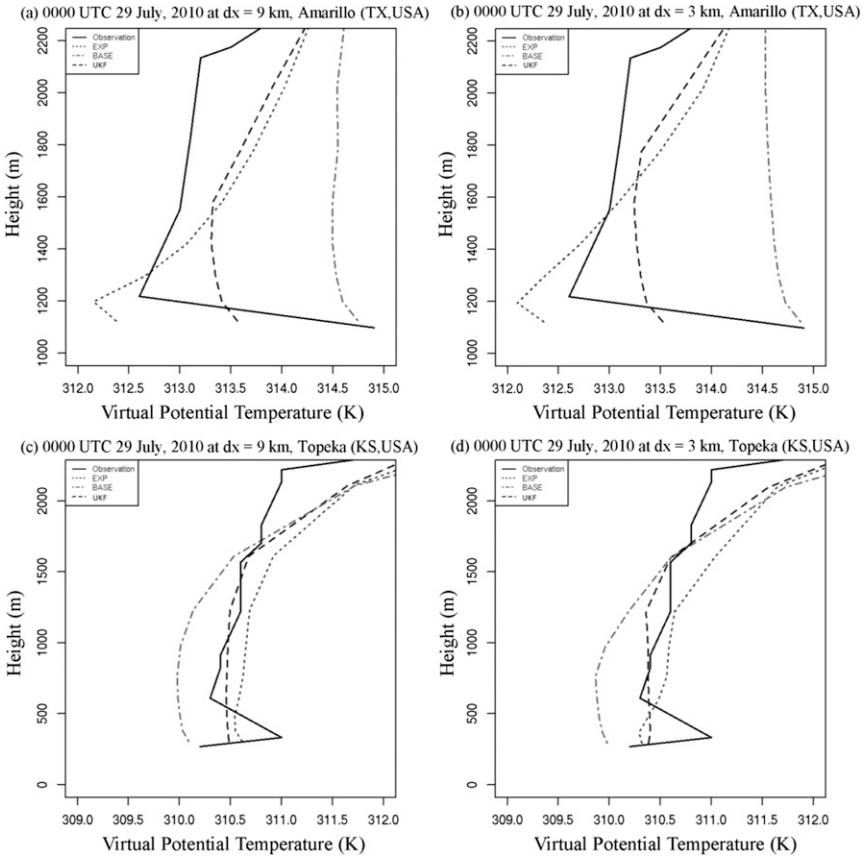

FIG. 11. Vertical profile of virtual potential temperature (K) at 0000 UTC 29 Jul 2010 at (a),(c) a 9-km grid spacing domain and (b),(d) a 3-km grid spacing domain valid at (top) Amarillo, TX (AMA, 35.23°N, 101.7°W), and (bottom) Topeka, KS (TOP, 39.07°N, 95.62°W).

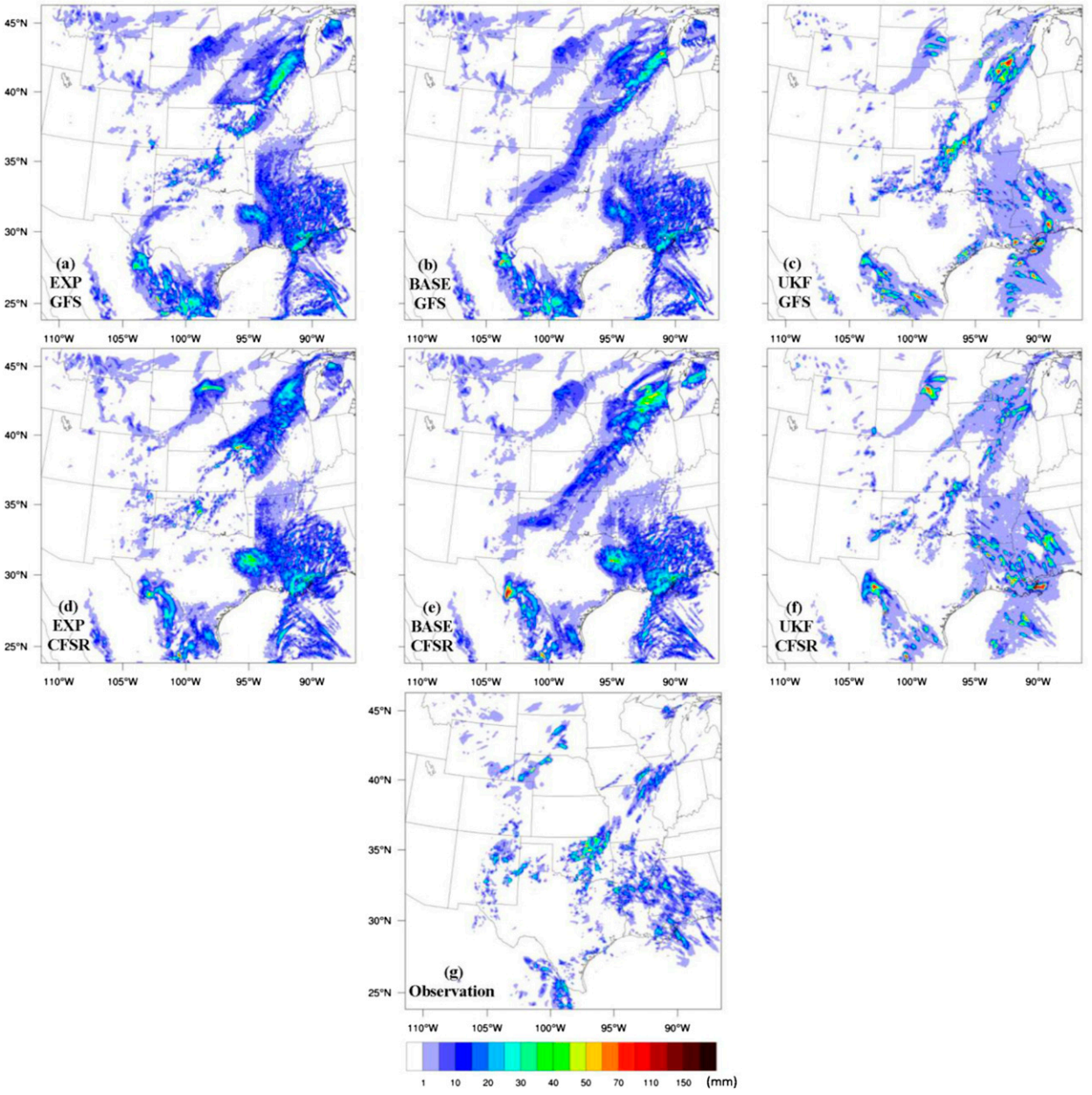

FIG. 12. Comparative example of simulated 6-h (1800 UTC 6 Jul–0000 UTC 7 Jul 2010) accumulated precipitation (mm) over a 9-km grid spacing domain with (top) GFS and (middle) CFSR for (a),(d) EXP; (b),(e) BASE; (c),(f) UKF; and (g) stage-IV observed precipitation.

influence of model initial conditions on the convection scheme's contribution to the precipitation forecast, suggesting that changes in the model initial conditions can have a direct effect on the simulation of precipitation through the convective parameterization used in NWP models.

Figure 11 shows the vertical profile of virtual potential temperature for two grid cells for the 9- and 3-km grid spacings at 0000 UTC 29 July 2010. Note that all three simulations miss the shallow surface inversion at TOP (39.07°N, 95.62°W) (Figs. 11c and 11d), and EXP and UKF underestimate the surface temperature at Amarillo, Texas (AMA, Figs. 11a and 11b). It is difficult to pick out whether EXP or UKF performed better at AMA (35.23°N, 101.7°W), since EXP looks slightly better in the lower levels and UKF performs best in the upper portion of the profile (Figs. 11a and 11b). Also note that the virtual potential temperatures for UKF are almost constant with height in the PBL and close to the observations from the International H_2O Project (IHOP), indicating

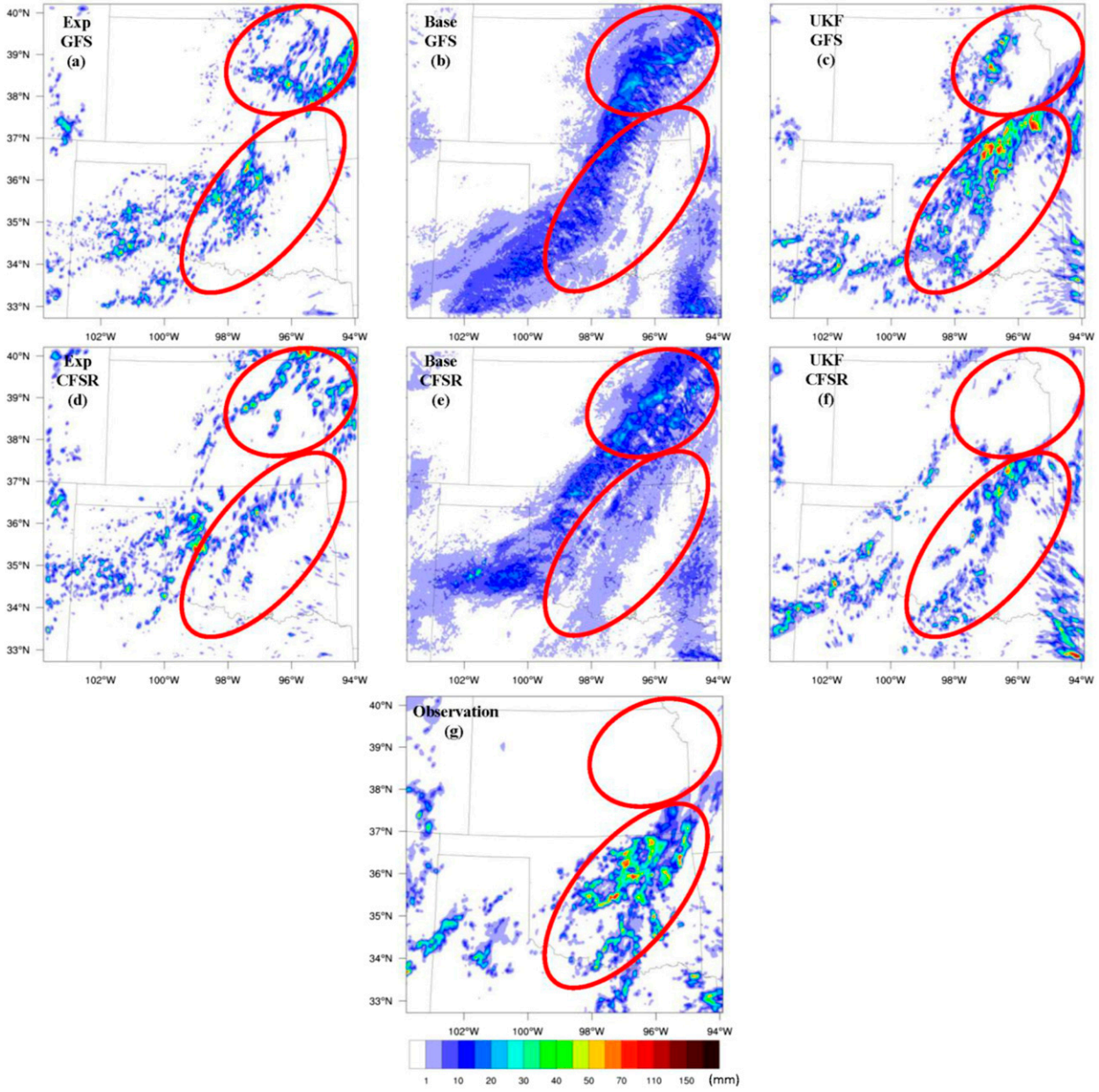

FIG. 13. Comparative example of simulated 6-h (1800 UTC 6 Jul–0000 UTC 7 Jul 2010) accumulated precipitation (mm) over a 3-km grid spacing domain with (top) GFS and (middle) CFSR for (a),(d) EXP; (b),(e) BASE; (c),(f) UKF; and (g) stage-IV observed precipitation.

that the MYJ scheme used in the WRF simulations with the updated KF scheme is capable of simulating improved well-mixed boundary layers.

c. Simulation period 0000 UTC 5 July–0000 UTC 7 July 2010: Experiments 13–18

A distinct widespread northeast–southwest rainfall was observed in Oklahoma during the local afternoon hours of 6 July 2010 (Figs. 12 and 13). Estimated 6-h (1800 UTC 5 July–0000 UTC 7 July 2010) accumulated precipitation for the EXP, BASE, and UKF simulations and the stage-IV observed precipitation are compared and shown in Figs. 12 and 13. In Fig. 12, the UKF scheme successfully reduced excessive rainfall produced by the BASE scheme. More interestingly, over the parent domain of EXP, scale separation issues with two-way nesting can be seen in the precipitation field as the convection scheme differs across the nest boundary (Figs. 12a and 12d). This boundary issue is alleviated by using the same convection scheme (as in

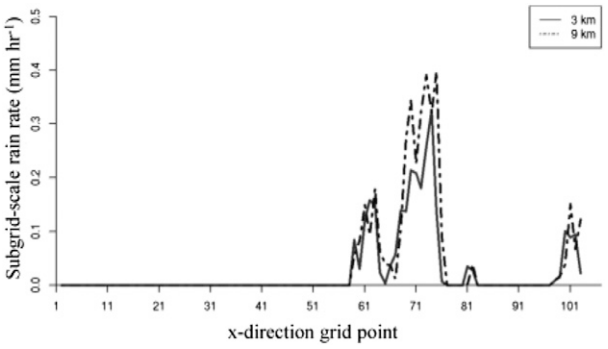

FIG. 14. The subgrid-scale rain rate (mm h^{-1}) simulated at 9- and 3-km grid spacings from the UKF scheme with GFS at 2000 UTC 5 Jul.

BASE or UKF) in the inner domain (Figs. 12b,c and 12e,f).

In the 3-km grid spacing simulations (Fig. 13), EXP forecasts more precipitation in northeast Kansas, while producing less precipitation than observed in Oklahoma. The improvement of using better initial conditions on high-resolution rainfall predictions can be seen in EXP and UKF, and at 3-km grid spacing, the precipitation simulated by UKF with GFS is similar to the stage-IV observation. However, the BASE run simulates more rainfall than observed and there are no obvious improvements when changing initial conditions. Since the UKF is able to improve the high-resolution precipitation forecast by introducing subgrid-scale effects, an instantaneous east–west-oriented transect of the subgrid-scale rain rate simulated at 9- and 3-km grid spacings is taken across Oklahoma and northern Texas at 2000 UTC 5 July 2010 (Fig. 14). It is found that the simulated convective rain rate for the finer-resolution model (i.e., 3-km grid spacing) is generally less than that for the coarser-resolution model (i.e., 9-km grid spacing) and confirms that subgrid-scale precipitation decreases when the model resolution increases.

d. *Sensitivity to microphysics schemes: Experiments 7–12 and 31–36*

Sensitivity analysis is useful for diagnosing the impacts of interactions of convective treatment and microphysics on regional forecasts of rainfall. A 48-h period starting at 0600 UTC 16 June 2002 during IHOP_2002 is examined due to significant convective activity and a large regional event that occurred over most of Oklahoma and large areas of Kansas and north Texas (Wilson and Roberts 2006). Sensitivity experiments (experiments 7–12 and 31–36 in Table 1) were conducted by varying model convective and microphysics schemes. The 6-h accumulated precipitation forecasts from all the experiments are compared to stage-IV precipitation analyses. Figure 15 provides an example of 9-km grid spacing forecasts of 6-h accumulated precipitation with the two microphysical parameterizations and three convective treatments. Since the outer domain is large compared to the inner domain, it mitigates the lateral boundary condition impacts on the inner domain. Figure 15 shows that the distributions of simulated precipitation vary significantly with different combinations of convective and microphysics schemes. Figure 16 shows an example of the sensitivity of precipitation to microphysical parameterization at 3-km grid spacing. The WDM6 scheme produces a large swath of precipitation with high values in the center. The Goddard scheme with UKF is not able to provide a large area of precipitation, although the orientation of the precipitation distribution is similar to observed rainfall. These results demonstrate that the impact of using the UKF scheme will vary from case to case and improvements may not be consistent with differing microphysics schemes. Therefore, for the cases where good initial conditions are not present, the microphysics scheme and the UKF scheme have limitations on improving the precipitation forecast.

e. *Sensitivity to each science update: Experiments 25–30*

We recall that the three updates that include properly representing the time scale (DYNTAU), grid-scale vertical velocity (WUP), and entrainment effect (ENT), have been employed to modify the original KF scheme, and as a result, the updated KF scheme has substantially reduced the excessive precipitation biases for NWP high-resolution forecasts. To find out which update is dominating the precipitation differences, six additional simulations (experiments 25–30 in Table 1) using each update separately initialized by GFS and CFSR were conducted for simulation period 0000 UTC 28 July–0000 UTC 30 July 2010. Figure 17 shows 48-h (0000 UTC 28 July–0000 UTC 30 July 2010) 3-km grid spacing area-averaged accumulated precipitation (mm) from stage-IV observations (black solid) and corresponding simulations in DYNTAU, WUP, ENT, UKF, and BASE using GFS (Fig. 17a) reanalysis data.

Since BASE produced more precipitation over wide areas as compared to the observation at 3-km grid spacing (Fig. 9), the simple area-averaged precipitation for BASE compensates its low precipitation intensity with an overprediction of areal rainfall coverage, resulting in better agreement of the area-averaged accumulated total precipitation with the observation. WUP slightly reduces the area-averaged total precipitation compared to BASE, indicating that the update with

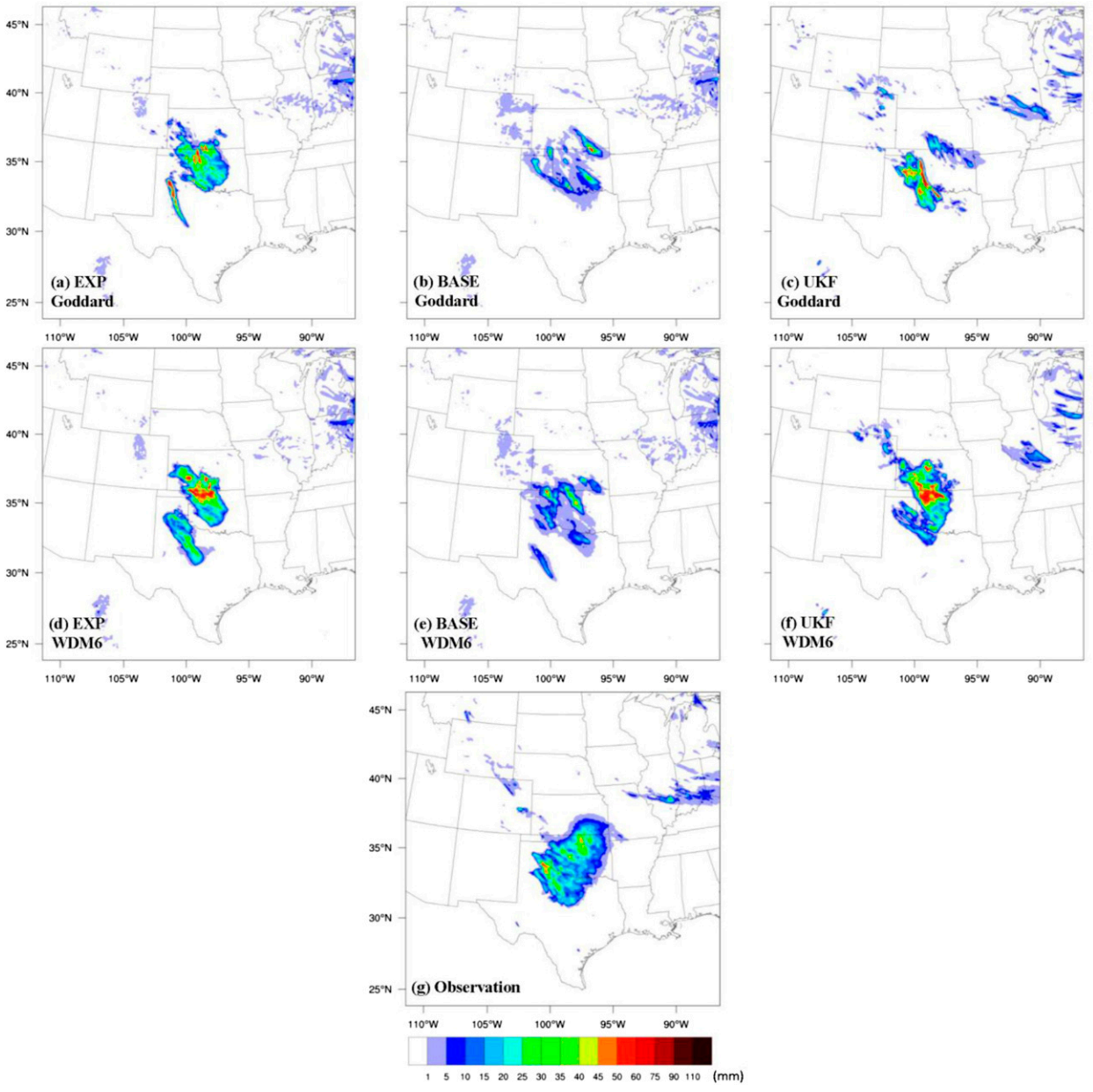

FIG. 15. Comparative example of simulated 6-h (0000–0600 UTC 16 Jun 2002) accumulated precipitation (mm) over a 9-km grid spacing domain with CFSR and (top) Goddard microphysics scheme and (middle) WRF double-moment 6-class scheme for the (a),(d) EXP; (b), (e) BASE; (c),(f) UKF; and (g) stage-IV observed precipitation.

subgrid-scale updraft mass flux impacts on grid-scale vertical velocity helps to slightly increase saturation levels of the environment, thereby leading to a minor increase in subgrid-scale precipitation. DYNTAU is found to contribute more to decreasing the simulated rainfall amount. One problem with many convective parameterization schemes is that as model resolution increases, impacts from a standard subgrid-scale parameterization become more significant. However, with the adjustment time scale τ update, the value of τ increases and results in longer time to remove CAPE for atmospheric stabilization, resulting in the simulated precipitation by DYNTAU being reduced, a desired feature. In the update of the entrainment effects, the introduced scale-dependent Tokioka parameter, as well as the LCL-based methodology, in the high-resolution simulation helps to achieve the proper representation of convective clouds through increased entrainment. As a

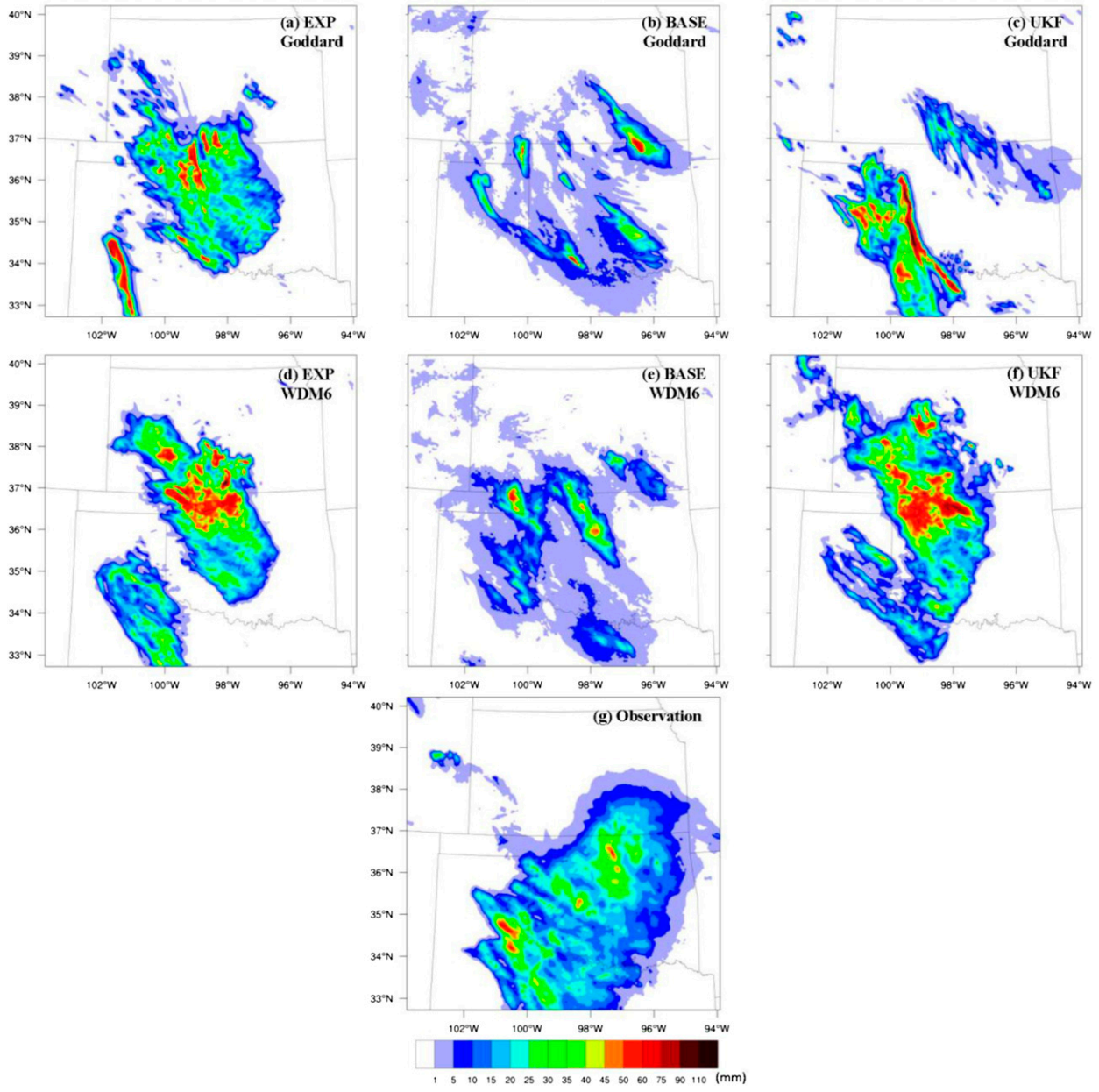

FIG. 16. Comparative example of simulated 6-h (0000–0600 UTC 16 Jun 2002) accumulated precipitation (mm) over a 3-km grid spacing domain with CFSR and (top) Goddard microphysics scheme and (middle) WRF double-moment 6-class scheme for (a),(d) EXP; (b),-(e) BASE; (c),(f) UKF; and (g) stage-IV observed precipitation.

result, the hyperactivity of the subgrid-scale convection scheme is alleviated, leading to a decrease of subgrid-scale precipitation. Consistently, ENT reduces the precipitation from BASE, and it shows the minimum area-averaged precipitation among all of the simulations with a separated update. To summarize, the three different updates contribute differently to the precipitation changes and show nonlinear impacts. We also found similar results using the CFSR reanalysis data (not shown). To further assess the relative contribution of each of the updates on precipitation components (i.e., subgrid scale versus grid scale), Fig. 17b shows 48-h accumulated subgrid-scale precipitation obtained from using each of the updates. In the literature, a few studies (e.g., Wang et al. 2009; Snively and Gallus 2014; Van Weverberg et al. 2013) use the term ''cloud permitting'' scale (quasi-convective resolution) for grid spacings that are smaller than 4 km. These studies demonstrate that

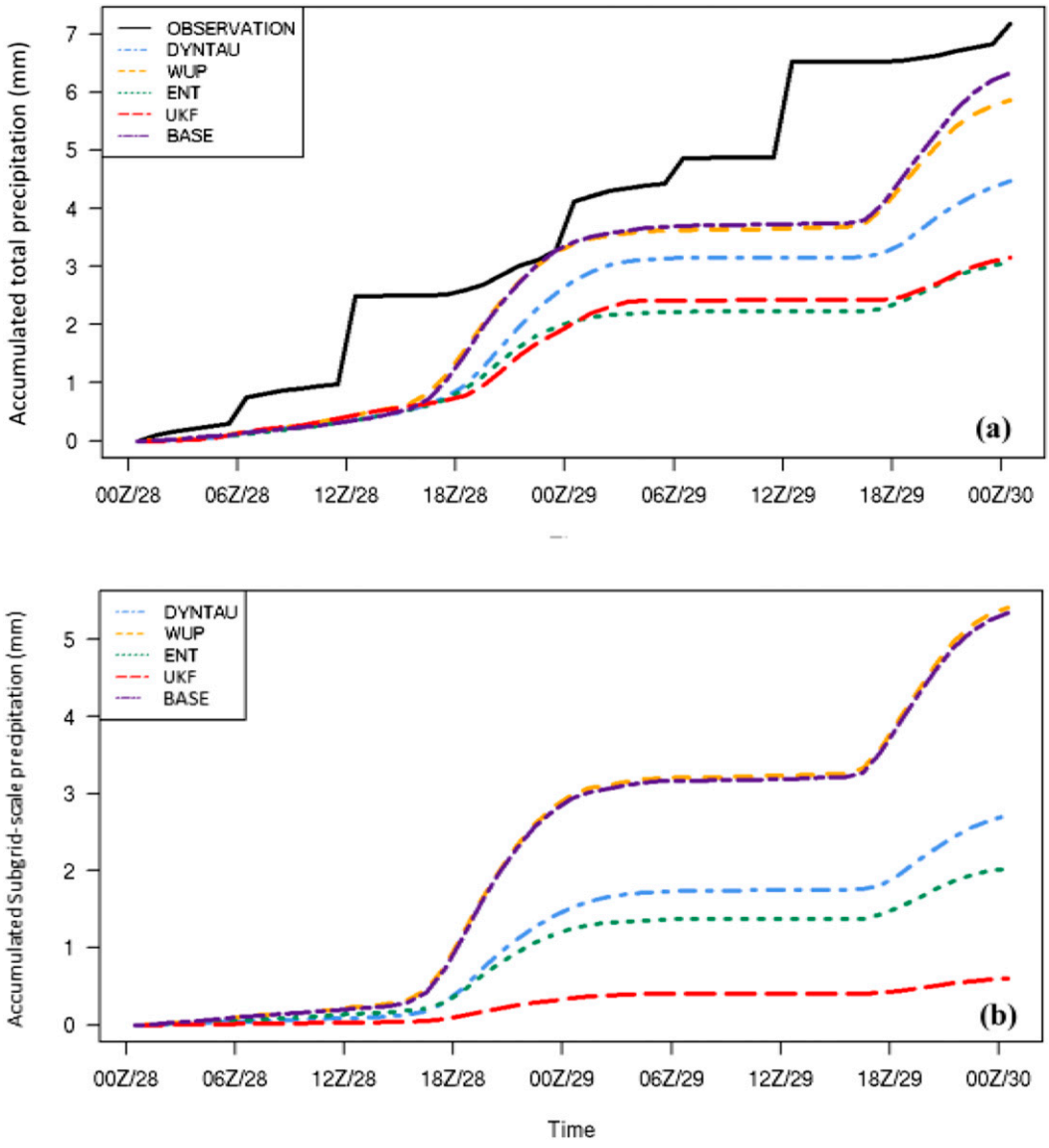

FIG. 17. The 48-h (0000 UTC 28 Jul–0000 UTC 30 Jul 2010) area averaged over 3-km grid spacing (a) accumulated total precipitation (mm) with GFS and (b) accumulated subgrid-scale precipitation (mm) with GFS: stage-IV observations (black solid) and corresponding simulations in DYNTAU (blue dot–dashed), WUP (orange dashed), ENT (green dotted), UKF (red long-dashed), and BASE (purple double dashed).

grid-scale microphysics schemes are adequate to produce reasonable precipitation in model forecasts/simulations at cloud-permitting scales, implying that the subgrid-scale convective component is either weak or absent. As shown by comparisons of Figs. 17a and 17b, the total precipitation in the UKF simulation is dominated by grid-scale precipitation, with the amount of subgrid rainfall below 1 mm for the entire forecast. To further examine relative intensity of precipitation with each of the updates, in Fig. 18 we present the accumulated value of 48-h (0000 UTC 28 July–0000 UTC 30 July 2010) 3-km grid spacing area-averaged precipitation (mm) from stage IV and corresponding simulations in DYNTAU, WUP, ENT, UKF, and BASE with GFS for certain thresholds of hourly rates. For the rate less than 5 mm h^{-1}, UKF slightly underpredicts while ENT is on average closest to the observations. Simulations with the other updates overpredict the observed rate. Results indicate that too much drizzle has been simulated by BASE and modifying the grid-scale vertical velocity alone cannot significantly improve the precipitation forecast. DYNTAU and ENT contribute to reduce the drizzle, and UKF, which includes

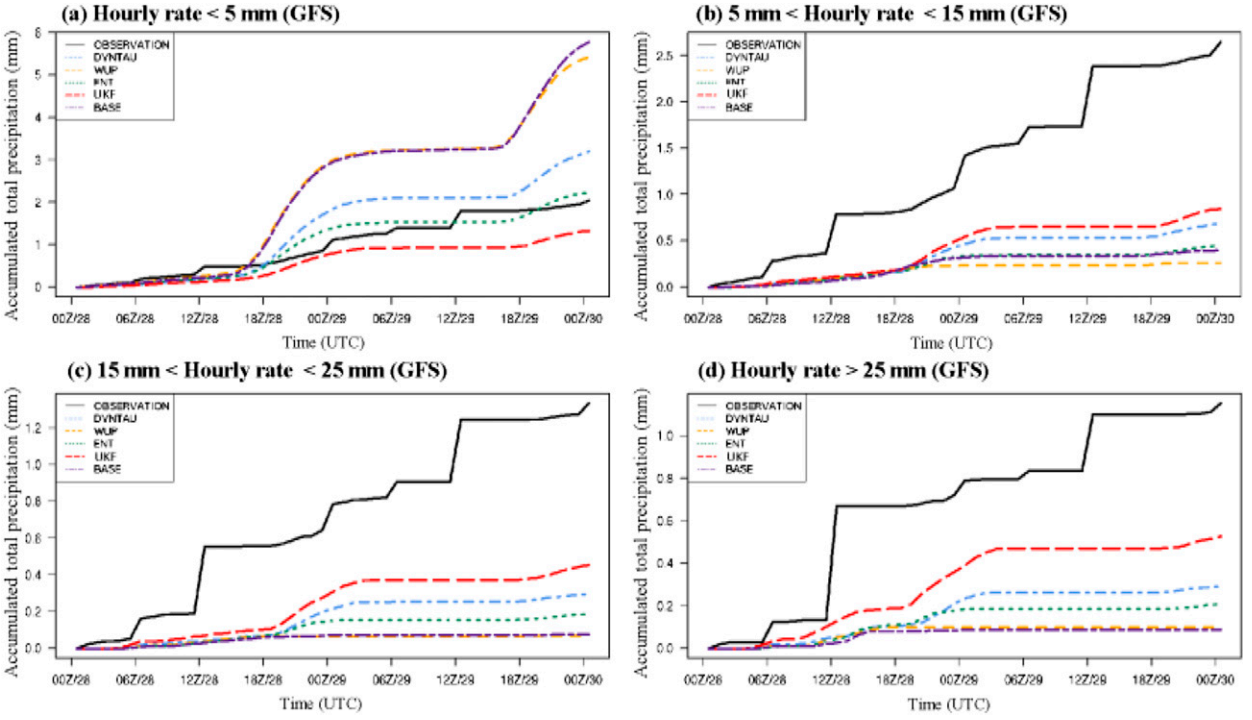

FIG. 18. The 48-h (0000 UTC 28 Jul–0000 UTC 30 Jul 2010) area averaged over 3-km grid spacing total precipitation (mm) from stage-IV observations (black solid) and corresponding simulations in DYNTAU (blue dot–dashed), WUP (orange dashed), ENT (green dotted), UKF (red long-dashed), and BASE (purple double dashed) with GFS.

all three updates, shows good improvement for the forecast of drizzle. But, for the rest of the hourly rates, UKF outperforms the other simulations. However, UKF still tends to underpredict precipitation values at rates greater than 5 mm h^{-1}. Figure 19 shows the accumulated 48-h (0000 UTC 28 July–0000 UTC 30 July 2010) area-averaged subgrid-scale precipitation (mm) for 3-km grid spacing from simulations in DYNTAU, WUP, ENT, UKF, and BASE with GFS when the hourly rates are in the same thresholds as shown in Fig. 18. It can be seen that UKF primarily contributes to the precipitation forecast when the rate is less than 5 mm h^{-1}, but negligibly improves the simulation when the rate is greater than 5 mm h^{-1} and less than 15 mm h^{-1}, and has zero contribution with higher hourly rain rates.

5. Summary and conclusions

The impacts of introducing parameterized cloud dynamics on high-resolution WRF Model forecasts were examined at 9- and 3-km grid spacing, simulating regional precipitation over the U.S. SGP with several cases of 48-h forecasts. An updated KF scheme, including subgrid-scale cloud–radiation interactions (Alapaty et al. 2012; Herwehe et al. 2014), a dynamic adjustment time scale, a simple linear method using cloud updraft mass fluxes impacting grid-scale vertical velocity, and a LCL-based methodology for parameterizing entrainment, was developed for high-resolution simulations and implemented in the WRF Model (version 3.4.1). The aforementioned parameters were adapted to be scale dependent, as shown in Eqs. (2), (5), and (9). Three cases of regional precipitation were selected and thirty-six 48-h WRF experiments that were made with three different treatments of convection (no cumulus convection representation, original KF, and updated KF) were initialized separately with two different initial conditions: the 1.0° 6-hourly GFS FNL dataset and 0.5° 6-hourly CFSR data. To determine the precipitation forecast sensitivity to microphysics and emphasize the importance of initial conditions, six model runs [which included the three different treatments of convection and two different microphysics schemes (Goddard and WDM6)], were initialized with CFSR. Overall, the updated KF scheme is found to generally improve the high-resolution simulation of longwave and shortwave radiation associated with cloud patterns, and produce precipitation patterns and intensity that are closer to the observations.

Experiments using GFS and CFSR for initialization were conducted to assess how the initial condition dataset impacts forecasts. These studies show that the general distribution and intensity of precipitation

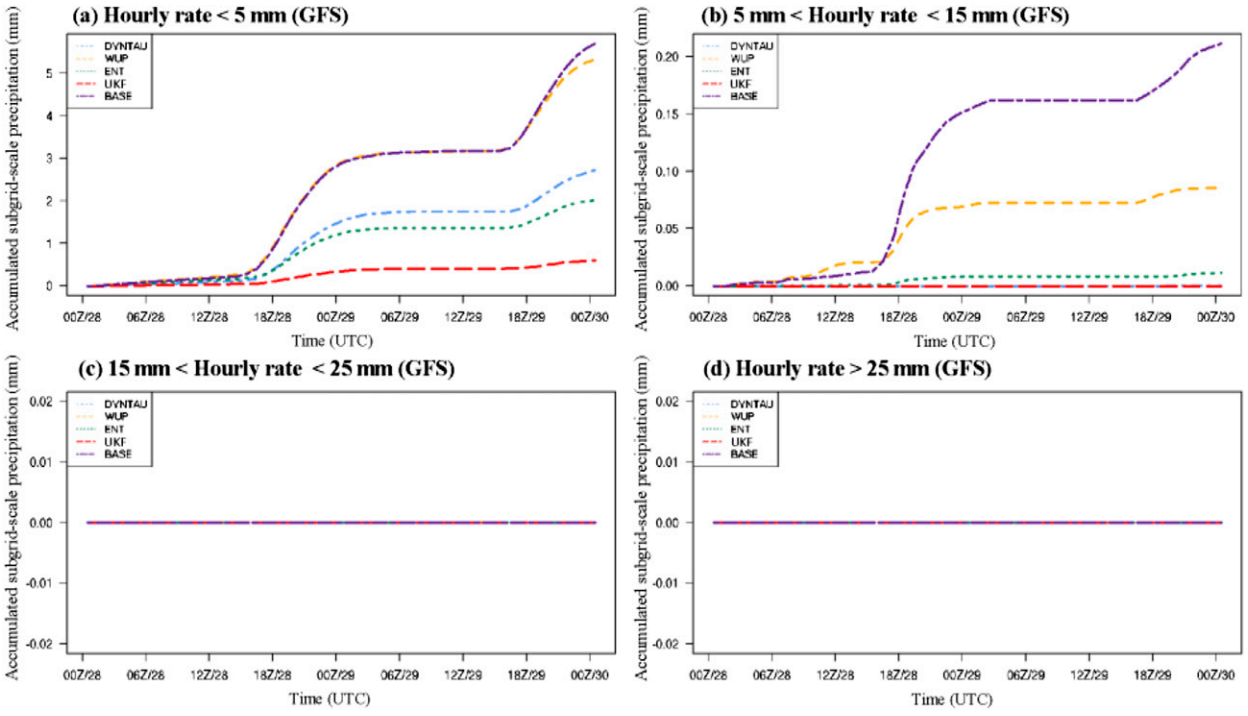

FIG. 19. The 48-h (0000 UTC 28 Jul–0000 UTC 30 Jul 2010) area averaged over 3-km grid spacing subgrid-scale precipitation (mm) from simulations in DYNTAU (blue dot–dashed), WUP (orange dashed), ENT (green dotted), UKF (red long-dashed), and BASE (purple double dashed) with GFS.

forecasts are significantly influenced by initial conditions obtained from different analysis fields. The area-averaged precipitation simulated using CFSR is found to be heavier compared to the GFS results. Simulations using the updated KF scheme outperform the other simulations at light, medium, and heavy precipitation rates, regardless of the dataset used for initial conditions. The larger differences in the area-averaged RMSE between the two initial conditions are found with the original KF scheme, but for heavy precipitation rates (greater than 25 mm h^{-1}), significant differences due to changes in initial conditions are noted in all of the convective treatments (Table 2). Sensitivity analysis demonstrates that the precipitation forecasts are more sensitive to the type of initialization than to grid-scale microphysics or convective treatments in our case studies. Therefore, a good initial condition dataset is necessary for a good NWP model forecast, consistent with that documented in the literature (Rabier et al. 1996; Stensrud et al. 2000; Ray et al. 2010; Pijanowski et al. 2011).

In this study we find that grid-resolution-dependent parameterized convective physics in the KF scheme results in improvement of high-resolution forecasts. Thus, the updated KF scheme in the WRF Model at high-resolution scales produces more accurate surface radiation values and results in the improvement of simulated cloudiness. The updated KF scheme not only reduces excessive rainfall amounts, but also improves both the location and intensity of precipitation in high-resolution (3- and 9-km grid spacing) forecasts. Regional climate simulations that are being performed by our group do indicate that each of the science updates presented in this paper results in a large reduction in monthly precipitation biases, which will be reported in a follow-up paper.

Acknowledgments. Parts of the research were funded by the U.S. EPA's Air, Climate, and Energy (ACE) Program, and USDA/NIFA Drought Triggers Grant 2011-67019-20042 through Texas A&M University, NSF Grants AGS-1522494 and CDS&E-1250232, and USDA NIFA Hatch Project 1007699 at Purdue University. Anthony Del Genio acknowledges support from the U.S. Department of Energy Atmospheric System Research Program. Our appreciation goes to Dr. John Kain of NOAA and Dr. Megan Mallard, Mr. Russell Bullock, Dr. Christopher Nolte, and Ms. Tanya Spero of the U.S. EPA for their help in many ways facilitating the research. This research has been subjected to the U.S. EPA's administrative review and approved for publication. The views expressed herein and the contents are solely the responsibility of the authors, and do not necessarily represent the official views of the U.S. EPA.

REFERENCES

Alapaty, K., J. A. Herwehe, T. L. Otte, C. G. Nolte, O. R. Bullock, M. S. Mallard, J. S. Kain, and J. Dudhia, 2012: Introducing subgrid-scale cloud feedbacks to radiation for regional meteorological and climate modeling. *Geophys. Res. Lett.*, **39**, L24809, doi:10.1029/2012GL054031.

Arakawa, A., and W. H. Schubert, 1974: Interaction of a cumulus cloud ensemble with the large-scale environment, Part I. *J. Atmos. Sci.*, **31**, 674–701, doi:10.1175/1520-0469(1974)031<0674:IOACCE>2.0.CO;2.

——, and J.-H. Jung, 2011: Multiscale modeling of the moist-convective atmosphere—A review. *Atmos. Res.*, **102**, 263–285, doi:10.1016/j.atmosres.2011.08.009.

——, and C.-M. Wu, 2013: A unified representation of deep moist convection in numerical modeling of the atmosphere. Part I. *J. Atmos. Sci.*, **70**, 1977–1992, doi:10.1175/JAS-D-12-0330.1.

Bechtold, P., M. Köhler, T. Jung, F. Doblas-Reyes, M. Leutbecher, M. J. Rodwell, F. Vitart, and G. Balsamo, 2008: Advances in simulating atmospheric variability with the ECMWF model: From synoptic to decadal time-scales. *Quart. J. Roy. Meteor. Soc.*, **134**, 1337–1351, doi:10.1002/qj.289.

Black, T. L., 1994: The new NMC mesoscale Eta model: Description and forecast examples. *Wea. Forecasting*, **9**, 265–278, doi:10.1175/1520-0434(1994)009<0265:TNNMEM>2.0.CO;2.

Blossey, P. N., C. S. Bretherton, J. Cetrone, and M. Kharoutdinov, 2007: Cloud-resolving model simulations of KWAJEX: Model sensitivities and comparisons with satellite and radar observations. *J. Atmos. Sci.*, **64**, 1488–1508, doi:10.1175/JAS3982.1.

Bryan, G. H., and H. Morrison, 2012: Sensitivity of a simulated squall line to horizontal resolution and parameterization of microphysics. *Mon. Wea. Rev.*, **140**, 202–225, doi:10.1175/MWR-D-11-00046.1.

Bullock, O. R., Jr., K. Alapaty, J. A. Herwehe, and J. S. Kain, 2015: A dynamically computed convective time scale for the Kain–Fritsch convective parameterization scheme. *Mon. Wea. Rev.*, **143**, 2105–2120, doi:10.1175/MWR-D-14-00251.1.

Case, J. L., W. L. Crosson, S. V. Kumar, W. M. Lapenta, and C. D. Peters-Lidard, 2008: Impacts of high-resolution land surface initialization on regional sensible weather forecasts from the WRF model. *J. Hydrometeor.*, **9**, 1249–1266, doi:10.1175/2008JHM990.1.

Chen, F., and Coauthors, 2011: The integrated WRF/urban modelling system: Development, evaluation, and applications to urban environmental problems. *Int. J. Climatol.*, **31**, 273–288, doi:10.1002/joc.2158.

——, and J. Dudhia, 2001: Coupling an advanced land surface hydrology model with the Penn State–NCAR MM5 modeling system. Part I: Model implementation and sensitivity. *Mon. Wea. Rev.*, **129**, 569–585, doi:10.1175/1520-0493(2001)129<0569:CAALSH>2.0.CO;2.

Chikira, M., and M. Sugiyama, 2010: A cumulus parameterization with state-dependent entrainment rate. Part I: Description and sensitivity to temperature and humidity profiles. *J. Atmos. Sci.*, **67**, 2171–2193, doi:10.1175/2010JAS3316.1.

Cintineo, R., J. A. Otkin, M. Xue, and F. Kong, 2014: Evaluating the performance of planetary boundary layer and cloud microphysical parameterization schemes in convection-permitting ensemble forecasts using synthetic *GOES-13* satellite observations. *Mon. Wea. Rev.*, **142**, 163–182, doi:10.1175/MWR-D-13-00143.1.

Clark, A. J., and Coauthors, 2012: An overview of the 2010 Hazardous Weather Testbed Experimental Forecast Program Spring Experiment. *Bull. Amer. Meteor. Soc.*, **93**, 55–74, doi:10.1175/BAMS-D-11-00040.1.

Dawson, D. T., M. Xue, J. A. Milbrandt, and M. K. Yau, 2010: Comparison of evaporation and cold pool development between single-moment and multimoment bulk microphysics schemes in idealized simulations of tornadic thunderstorms. *Mon. Wea. Rev.*, **138**, 1152–1171, doi:10.1175/2009MWR2956.1.

de Rooy, W. C., and Coauthors, 2013: Entraiment and detrainment in cumulus convection: An overview. *Quart. J. Roy. Meteor. Soc.*, **139**, 1–19, doi:10.1002/qj.1959.

Del Genio, A. D., and J. Wu, 2010: The role of entrainment in the diurnal cycle of continental convection. *J. Climate*, **23**, 2722–2738, doi:10.1175/2009JCLI3340.1.

——, Y. Chen, D. Kim, and M.-S. Yao, 2012: The MJO transition from shallow to deep convection in *CloudSat/CALIPSO* data and GISS GCM simulations. *J. Climate*, **25**, 3755–3770, doi:10.1175/JCLI-D-11-00384.1.

Deng, A., and D. R. Stauffer, 2006: On improving 4-km mesoscale model simulations. *J. Appl. Meteor. Climatol.*, **45**, 361–381, doi:10.1175/JAM2341.1.

Done, J. M., C. A. Davis, and M. Weisman, 2004: The next generation of NWP: Explicit forecasts of convection using the Weather Research and Forecasting (WRF) model. *Atmos. Sci. Lett.*, **5**, 110–117, doi:10.1002/asl.72.

——, G. C. Craig, S. L. Gray, P. A. Clark, and M. E. B. Gray, 2006: Mesoscale simulations of organized convection: Importance of convective equilibrium. *Quart. J. Roy. Meteor. Soc.*, **132**, 737–756, doi:10.1256/qj.04.84.

Ehrendorfer, M., 1997: Predicting the uncertainty of numerical weather forecasts: A review. *Meteor. Z.*, **6**, 147–183.

Fritsch, J. M., and C. F. Chappell, 1980: Numerical prediction of convectively driven mesoscale pressure systems. Part I: Convective parameterization. *J. Atmos. Sci.*, **37**, 1722–1733, doi:10.1175/1520-0469(1980)037<1722:NPOCDM>2.0.CO;2.

Grant, A. L. M., and A. P. Lock, 2004: The turbulent kinetic energy budget for shallow cumulus convection. *Quart. J. Roy. Meteor. Soc.*, **130**, 401–422, doi:10.1256/qj.03.50.

Gustafson, W. I., Jr., P.-L. Ma, H. Xiao, B. Singh, P. J. Rasch, and J. D. Fast, 2013: The Separate Physics and Dynamics Experiment (SPADE) framework for determining resolution awareness: A case study of microphysics. *J. Geophys. Res. Atmos.*, **118**, 9258–9276, doi:10.1002/jgrd.50711.

Han, J., and H.-L. Pan, 2011: Revision of convection and vertical diffusion schemes in the NCEP Global Forecast System. *Wea. Forecasting*, **26**, 520–533, doi:10.1175/WAF-D-10-05038.1.

Herwehe, J. A., K. Alapaty, T. L. Spero, and C. G. Nolte, 2014: Increasing the credibility of regional climate simulations by introducing subgrid-scale cloud–radiation interactions. *J. Geophys. Res. Atmos.*, **119**, 5317–5330, doi:10.1002/2014JD021504.

Holland, J. Z., and E. M. Rasmusson, 1973: Measurement of atmospheric mass, energy, and momentum budgets over a 500-kilometer square of tropical ocean. *Mon. Wea. Rev.*, **101**, 44–55, doi:10.1175/1520-0493(1973)101<0044:MOTAME>2.3.CO;2.

Holt, T. R., D. Niyogi, F. Chen, K. Manning, M. A. LeMone, and A. Qureshi, 2006: Effect of land–atmosphere interactions on the IHOP 24–25 May 2002 convection case. *Mon. Wea. Rev.*, **134**, 113–133, doi:10.1175/MWR3057.1.

Hong, S.-Y., J. Dudhia, and S.-H. Chen, 2004: A revised approach to ice microphysical processes for the bulk parameterization of clouds and precipitation. *Mon. Wea. Rev.*, **132**, 103–120, doi:10.1175/1520-0493(2004)132<0103:ARATIM>2.0.CO;2.

——, K.-S. Sunny Lim, Y.-H. Lee, J.-C. Ha, H.-W. Kim, S.-J. Ham, and J. Dudhia, 2010: Evaluation of the WRF double-moment 6-class microphysics scheme for precipitating convection. *Adv. Meteor.*, **2010**, 707253, doi:10.1155/2010/707253.

Houghton, H., and H. Cramer, 1951: A theory of entrainment in convective currents. *J. Meteor.*, **8**, 95–102, doi:10.1175/1520-0469(1951)008<0095:ATOEIC>2.0.CO;2.

Iacono, M. J., J. S. Delamere, E. J. Mlawer, M. W. Shepard, S. A. Clough, and W. D. Collins, 2008: Radiative forcing by long-lived greenhouse gases: Calculations with the AER radiative transfer models. *J. Geophys. Res.*, **113**, D13103, doi:10.1029/2008JD009944.

Janjić, Z. I., 2002: Nonsingular implementation of the Mellor–Yamada level 2.5 scheme in the NCEP Meso model. NCEP Office Note 437, 61 pp.

Kain, J. S., 2004: The Kain–Fritsch convective parameterization: An update. *J. Appl. Meteor.*, **43**, 170–181, doi:10.1175/1520-0450(2004)043<0170:TKCPAU>2.0.CO;2.

——, and J. M. Fritsch, 1990: A one-dimensional entraining/detraining plume model and its application in convective parameterization. *J. Atmos. Sci.*, **47**, 2784–2802, doi:10.1175/1520-0469(1990)047<2784:AODEPM>2.0.CO;2.

——, and ——, 1993: Convective parameterization for mesoscale models: The Kain–Fritsch scheme. *The Representation of Cumulus Convection in Numerical Models*, *Meteor. Monogr.*, No. 24, Amer. Meteor. Soc., 165–170.

——, and Coauthors, 2008: Some practical considerations regarding horizontal resolution in the first generation of operational convection-allowing NWP. *Wea. Forecasting*, **23**, 931–952, doi:10.1175/WAF2007106.1.

Kang, S. M., D. M. W. Frierson, and I. M. Held, 2009: The tropical response to extratropical thermal forcing in an idealized GCM: The importance of radiative feedbacks and convective parameterization. *J. Atmos. Sci.*, **66**, 2812–2827, doi:10.1175/2009JAS2924.1.

Kim, D., A. H. Sobel, E. D. Maloney, D. M. W. Frierson, and I.-S. Kang, 2011: A systematic relationship between intraseasonal variability and mean state bias in AGCM simulations. *J. Climate*, **24**, 5506–5520, doi:10.1175/2011JCLI4177.1.

Koster, R. D., and Coauthors, 2004: Regions of strong coupling between soil moisture and precipitation. *Science*, **305**, 1138–1140, doi:10.1126/science.1100217.

Lawrence, M. G., and P. J. Rasch, 2005: Tracer transport in deep convective updrafts: Plume ensemble versus bulk formulations. *J. Atmos. Sci.*, **62**, 2880–2894, doi:10.1175/JAS3505.1.

LeMone, M. A., and Coauthors, 2007: NCAR/CU surface, soil, and vegetation observations during the International H_2O Project 2002 field campaign. *Bull. Amer. Meteor. Soc.*, **88**, 65–81, doi:10.1175/BAMS-88-1-65.

Lin, Y., and K. E. Mitchell, 2005: The NCEP Stage II/IV hourly precipitation analyses: Development and applications. *19th Conf. on Hydrology*, San Diego, CA, Amer. Meteor. Soc., 1.2. [Available online at https://ams.confex.com/ams/Annual2005/techprogram/paper_83847.htm.]

——, M. Zhao, Y. Ming, J.-C. Golaz, L. J. Donner, S. A. Klein, V. Ramaswamy, and S. Xie, 2013: Precipitation partitioning, tropical clouds, and intraseasonal variability in GFDL AM2. *J. Climate*, **26**, 5453–5466, doi:10.1175/JCLI-D-12-00442.1.

Luo, Y., Y. Wang, H. Wang, Y. Zheng, and H. Morrison, 2010: Modeling convective-stratiform precipitation processes on a Mei-Yu front with the Weather Research and Forecasting model: Comparison with observations and sensitivity to cloud microphysics parameterizations. *J. Geophys. Res.*, **115**, D18117, doi:10.1029/2010JD013873.

Mallard, M. S., G. M. Lackmann, A. Aiyyer, and K. Hill, 2013: Atlantic hurricanes and climate change. Part I: Experimental design and isolation of thermodynamic effects. *J. Climate*, **26**, 4876–4893, doi:10.1175/JCLI-D-12-00182.1.

Mishra, S. K., and J. Srinivasan, 2010: Sensitivity of the simulated precipitation to changes in convective relaxation time scale. *Ann. Geophys.*, **28**, 1827–1846, doi:10.5194/angeo-28-1827-2010.

Molinari, J., and M. Dudek, 1992: Parameterization of convective precipitation in mesoscale numerical models: A critical review. *Mon. Wea. Rev.*, **120**, 326–344, doi:10.1175/1520-0493(1992)120<0326:POCPIM>2.0.CO;2.

Neale, R. B., and Coauthors, 2010: Description of the NCAR Community Atmospheric Model (CAM5.0). NCAR Tech. Note NCAR/TN-486+STR, 268 pp. [Avalable online at http://www.cesm.ucar.edu/models/cesm1.0/cam/docs/description/cam5_desc.pdf.]

Niyogi, D., P. Pyle, M. Lei, S. P. Arya, C. M. Kishtawal, M. Shepherd, F. Chen, and B. Wolfe, 2011: Urban modification of thunderstorms: An observational storm climatology and model case study for the Indianapolis urban region. *J. Appl. Meteor. Climatol.*, **50**, 1129–1144, doi:10.1175/2010JAMC1836.1.

Otte, T. L., C. G. Nolte, M. J. Otte, and J. H. Bowden, 2012: Does nudging squelch the extremes in regional climate modeling? *J. Climate*, **25**, 7046–7066, doi:10.1175/JCLI-D-12-00048.1.

Pijanowski, B., N. Moore, D. Mauree, and D. Niyogi, 2011: Evaluating error propagation in coupled land–atmosphere models. *Earth Interact.*, **15**, doi:10.1175/2011EI380.1.

Rabier, F., E. Klinker, P. Courtier, and A. Hollingsworth, 1996: Sensitivity of forecast errors to initial conditions. *Quart. J. Roy. Meteor. Soc.*, **122**, 121–150, doi:10.1002/qj.49712252906.

Ray, D. K., R. A. Pielke, U. S. Nair, and D. Niyogi, 2010: Roles of atmospheric and land surface data in dynamic regional downscaling. *J. Geophys. Res.*, **115**, D05102, doi:10.1029/2009JD012218.

Richter, J. H., and P. J. Rasch, 2008: Effects of convective momentum transport on the atmospheric circulation in the Community Atmosphere Model, version 3. *J. Climate*, **21**, 1487–1499, doi:10.1175/2007JCLI1789.1.

Romps, D. M., and Z. Kuang, 2010: Do undiluted convective plumes exist in the upper tropical troposphere? *J. Atmos. Sci.*, **67**, 468–484, doi:10.1175/2009JAS3184.1.

Seaman, N. L., S. A. Michelson, P. C. Shafran, and D. R. Stauffer, 1998: Forecast of a severe squall line development in MM5 using explicit moist physics at 4-km resolution. Preprints, *12th Conf. on Numerical Weather Prediction*, Phoenix, AZ, Amer. Meteor. Soc., J1–J4.

Seifert, A., and B. Stevens, 2010: Microphysical scaling relations in a kinematic model of isolated shallow cumulus clouds. *J. Atmos. Sci.*, **67**, 1575–1590, doi:10.1175/2009JAS3319.1.

Simmons, A. J., and A. Hollingsworth, 2002: Some aspects of the improvement in skill of numerical weather prediction. *Quart. J. Roy. Meteor. Soc.*, **128**, 647–677, doi:10.1256/003590002321042135.

Skamarock, W. C., and J. B. Klemp, 2008: A time-split nonhydrostatic atmospheric model for weather research and forecasting applications. *J. Comput. Phys.*, **227**, 3465–3485, doi:10.1016/j.jcp.2007.01.037.

——, ——, M. G. Duda, L. D. Fowler, S.-H. Park, and T. D. Ringler, 2012: A multiscale nonhydrostatic atmospheric model using centroidal Voronoi tesselations and C-grid staggering. *Mon. Wea. Rev.*, **140**, 3090–3105, doi:10.1175/MWR-D-11-00215.1.

Snively, D. V., and W. A. Gallus Jr., 2014: Prediction of convective morphology in near-cloud-permitting WRF model

simulations. *Wea. Forecasting*, **29**, 130–149, doi:10.1175/WAF-D-13-00047.1.

Stensrud, D. J., 2007: *Parameterization Schemes: Keys to Understanding Numerical Weather Prediction Models.* Cambridge University Press, 462 pp.

——, J. Bao, and T. T. Warner, 2000: Using initial condition and model physics perturbations in short-range ensemble simulations of mesoscale convective systems. *Mon. Wea. Rev.*, **128**, 2077–2107, doi:10.1175/1520-0493(2000)128<2077:UICAMP>2.0.CO;2.

Stevens, D. E., and C. S. Bretherton, 1999: Effects of resolution on the simulation of stratocumulus entrainment. *Quart. J. Roy. Meteor. Soc.*, **125**, 425–439, doi:10.1002/qj.49712555403.

Tao, W. K., J. Simpson, and M. McCumber, 1989: An ice-water saturation adjustment. *Mon. Wea. Rev.*, **117**, 231–235, doi:10.1175/1520-0493(1989)117<0231:AIWSA>2.0.CO;2.

Tokioka, T., K. Yamazaki, A. Kotoh, and T. Ose, 1988: The equatorial 30-60 day oscillation and the Arakawa–Schubert penetrative cumulus parameterization. *J. Meteor. Soc. Japan*, **66**, 883–900.

van Lier-Walqui, M., T. Vukicevic, and D. J. Posselt, 2012: Quantification of cloud microphysical parameterization uncertainty using radar reflectivity. *Mon. Wea. Rev.*, **140**, 3442–3466, doi:10.1175/MWR-D-11-00216.1.

Van Weverberg, K., and Coauthors, 2013: The role of cloud microphysics parameterization in the simulation of mesoscale convective system clouds and precipitation in the tropical western Pacific. *J. Atmos. Sci.*, **70**, 1104–1128, doi:10.1175/JAS-D-12-0104.1.

Wang, W., and N. L. Seaman, 1997: A comparison of convective parameterization schemes in a mesoscale model. *Mon. Wea. Rev.*, **125**, 252–278, doi:10.1175/1520-0493(1997)125<0252:ACSOCP>2.0.CO;2.

Wang, X., H. Xie, H. Sharif, and J. Zeitler, 2008: Validating NEXRAD MPE and stage III precipitation products for uniform rainfall on the Upper Guadalupe River Basin of the Texas Hill Country. *J. Hydrol.*, **348**, 73–86, doi:10.1016/j.jhydrol.2007.09.057.

Wang, Y., C. N. Long, L. R. Leung, J. Dudhia, S. A. McFarlane, J. H. Mather, S. J. Ghan, and X. Liu, 2009: Evaluating regional cloud-permitting simulations of the WRF model for the Tropical Warm Pool International Cloud Experiment (TWP-ICE) Darwin, 2006. *J. Geophys. Res.*, **114**, D21203, doi:10.1029/2009JD012729.

Weisman, M. L., C. Davis, W. Wang, K. W. Manning, and J. B. Klemp, 2008: Experiences with 0–36-h explicit convective forecasts with the WRF-ARW model. *Wea. Forecasting*, **23**, 407–437, doi:10.1175/2007WAF2007005.1.

Westcott, N. E., 2009: Differences in multi-sensor and rain-gauge precipitation amounts. *Water Manage.*, **162**, 73–81.

——, H. V. Knapp, and S. D. Hilberg, 2008: Comparison of gage and multi-sensor precipitation estimates over a range of spatial and temporal scales in the Midwestern United States. *J. Hydrol.*, **351**, 1–12, doi:10.1016/j.jhydrol.2007.10.057.

Wilson, J. W., and R. D. Roberts, 2006: Summary of convective storm initiation and evolution during IHOP: Observational and modeling perspective. *Mon. Wea. Rev.*, **134**, 23–47, doi:10.1175/MWR3069.1.

Wulfmeyer, V., H.-S. Bauer, M. Grzeschik, A. Behrendt, F. Vandenberghe, E. V. Browell, S. Ismail, and R. A. Ferrare, 2006: Four-dimensional variational assimilation of water vapor differential absorption lidar data: The first case study within IHOP_2002. *Mon. Wea. Rev.*, **134**, 209–230, doi:10.1175/MWR3070.1.

Zhang, G. J., and N. A. McFarlane, 1995: Sensitivity of climate simulations to the parameterization of cumulus convection in the Canadian Climate Center general circulation model. *Atmos.–Ocean*, **33**, 407–446, doi:10.1080/07055900.1995.9649539.

Zheng, Y., A. Kumar, and D. Niyogi, 2015: Impacts of land–atmosphere coupling on regional rainfall and convection. *Climate Dyn.*, **44**, 2383–2409, doi:10.1007/s00382-014-2442-8.